Mineralogical Magazine (2024), **88**, 228–243
doi:10.1180/mgm.2023.98

CAMBRIDGE UNIVERSITY PRESS

Article

Heflikite, ideally $Ca_2(Al_2Sc)(Si_2O_7)(SiO_4)O(OH)$, the first scandium epidote-supergroup mineral from Jordanów Śląski, Lower Silesia, Poland and from Heftetjern, Tørdal, Norway

Adam Pieczka[1], Roy Kristiansen[2], Marcin Stachowicz[3], Magdalena Dumańska-Słowik[1], Bożena Gołębiowska[1], Mateusz P. Sęk[1], Krzysztof Nejbert[3], Jakub Kotowski[3], Beata Marciniak-Maliszewska[3], Adam Szuszkiewicz[4], Eligiusz Szełęg[5] and Krzysztof Woźniak[6]

[1]Department of Mineralogy, Petrography and Geochemistry, AGH University of Krakow, Mickiewicza 30, 30-059 Kraków, Poland; [2]Retired chemical engineer, N-1650 Sellebakk, Norway; [3]Faculty of Geology, University of Warsaw, 02-089 Warszawa, Żwirki and Wigury 93, Poland; [4]Institute of Geological Sciences, University of Wrocław, 50-204 Wrocław, M. Borna 9, Poland; [5]Department of Geochemistry, Mineralogy and Petrography, University of Silesia, 41-200 Sosnowiec, Będzińska 60, Poland; and [6]Department of Chemistry, University of Warsaw, 02-093 Warszawa, Pasteura 1, Poland

Abstract

Heflikite, the first Sc-dominant epidote-supergroup mineral, was discovered in two occurrences. The holotype was found in a granitic pegmatite associated with rodingite-like calc-silicate rocks and metasomatised granitic bodies exposed in a serpentinite quarry at Jordanów Śląski near Sobótka, Lower Silesia, SW Poland. The cotype comes from the Heftetjern pegmatite, Tørdal region, Norway. The holotype is composed of (in wt.%): 35.69 SiO_2, 0.22 TiO_2, 21.98 Al_2O_3, 6.12 Sc_2O_3, 0.07 V_2O_3, 1.10 Fe_2O_3, 0.11 Y_2O_3, 1.55 La_2O_3, 4.05 Ce_2O_3, 0.31 Pr_2O_3, 1.53 Nd_2O_3, 0.40 Sm_2O_3, 0.11 EuO, 0.56 Gd_2O_3, 0.14 MnO, 3.56 FeO, 0.16 MgO, 19.16 CaO and 1.78 $H_2O^{(+)}_{calc.}$; total 98.60. The cotype contains: 34.92 SiO_2, 0.44 TiO_2, 0.82 SnO_2, 19.13 Al_2O_3, 4.79 Sc_2O_3, 1.96 Fe_2O_3, 2.55 La_2O_3, 7.39 Ce_2O_3, 0.48 Pr_2O_3, 0.67 Nd_2O_3, 0.12 EuO, 0.61 Gd_2O_3, 0.13 MnO, 5.97 FeO, 17.66 CaO and 1.73 $H_2O^{(+)}_{calc.}$; total 99.37. The compositions correspond to the following empirical formulae: $(Ca_{1.729}Ce_{0.125}La_{0.048}Nd_{0.046}Gd_{0.016}Sm_{0.012}Pr_{0.010}Y_{0.005}Eu^{2+}_{0.003})_{\Sigma 1.994}[(Al_{2.182}Sc_{0.449}Fe^{3+}_{0.070}V^{3+}_{0.005})_{\Sigma 2.706}(Fe^{2+}_{0.251}Mg_{0.020}Mn_{0.010})_{\Sigma 0.281}Ti_{0.014}]_{\Sigma 3.001}(Si_{3.006}O_{11})O(OH)$ and $(Ca_{1.644}Ce_{0.235}La_{0.082}Nd_{0.021}Gd_{0.018}Pr_{0.015}Eu^{2+}_{0.004})_{\Sigma 1.019}[(Al_{1.958}Sc_{0.362}Fe^{3+}_{0.128})_{\Sigma 2.448}(Fe^{2+}_{0.434}Mn_{0.009})_{\Sigma 0.443}(Ti_{0.029}Sn_{0.029})_{\Sigma 0.058}]_{\Sigma 2.949}(Si_{3.033}O_{11})O(OH)$, respectively, and to the ideal formula $Ca_2(Al_2Sc)(Si_2O_7)(SiO_4)O(OH)$. The crystal structure of the holotype was refined in the monoclinic system with an R_1 index of 8.62%. The crystal-structure refinement indicates exclusively Si occupied T sites, Al occupied M1 and M2 sites, and a Ca occupied A1 site. The M3 site is filled predominantly by trivalent cations, mainly Sc^{3+}, with divalent cations (mainly Fe^{2+}) as minor occupants. The A2 site is filled mostly by Ca with minor amounts of rare earth elements (REE). The holotype heflikite crystallised from metasomatic fluids that infiltrated a contact between the granitic pegmatite and the surrounding rodingite-type calc-silicate rocks and serpentinites. The fluids that introduced Sc into the pegmatite could have been either hydrothermal or related to low-grade regional metamorphism that postdated the formation of the pegmatite. The cotype heflikite formed during the late-stage hydrothermal crystallisation of the Sc-enriched granitic pegmatite.

Keywords: scandium; epidote group; new mineral; heflikite; composition; crystal-structure refinement; Jordanów Śląski; Poland; Heftetjern pegmatite; Norway

(Received 9 July 2023; accepted 22 December 2023; Accepted Manuscript published online: 12 January 2024; Associate Editor: Mihoko Hoshino)

Introduction

The presence of scandium in epidote-supergroup minerals is very poorly documented in the scientific literature. In routine petrological studies these minerals are not usually tested for the presence of this element. Frei *et al.* (2004) reviewed the available data and concluded that although epidote-supergroup minerals seem to be enriched in Sc compared to their host rocks, there is no compelling evidence that natural Sc-rich epidotes exist. To the best of our knowledge, the only reports on epidote-supergroup minerals with significant contents of Sc concern allanite-group minerals, i.e. dissakisite-(Ce) with up to 1.0 wt.% Sc_2O_3 from a pegmatite at Impilakhti, Finland (Meyer, 1911) and allanite-(Ce) with up to 0.5 wt.% Sc_2O_3 from the Crystal Mountains, Montana, USA (Foord *et al.*, 1993), 2–5 wt.% Sc_2O_3 from the Heftetjern pegmatite, Norway (Raade and Kristiansen, 2000; Kristiansen, 2009), and up to 3.26 wt.% Sc_2O_3 from the Kracovice pegmatite,

Corresponding author: Adam Pieczka; Email: pieczka@agh.edu.pl
Cite this article: Pieczka A., Kristiansen R., Stachowicz M., Dumańska-Słowik M., Gołębiowska B., Sęk M.P., Nejbert K., Kotowski J., Marciniak-Maliszewska B., Szuszkiewicz A., Szełęg E. and Woźniak K. (2024) Heflikite, ideally $Ca_2(Al_2Sc)(Si_2O_7)(SiO_4)O(OH)$, the first scandium epidote-supergroup mineral from Jordanów Śląski, Lower Silesia, Poland and from Heftetjern, Tørdal, Norway. *Mineralogical Magazine* **88**, 228–243. https://doi.org/10.1180/mgm.2023.98

Moldanubian Zone, Czech Republic (Čopjaková *et al.*, 2015). Recently, during a systematic investigation of Sc mineralisation in a serpentinite-hosted granitic pegmatite at Jordanów Śląski, Lower Silesia, Poland, Sc-enriched epidote-supergroup minerals containing up to 9.54 wt.% Sc_2O_3 were discovered. In the Jordanów Śląski pegmatite, crystals with the highest Sc contents represent a Sc-analogue of clinozoisite and epidote, which has been approved by the Commission on New Minerals, Nomenclature and Classification of the International Mineralogical Association under the name heflikite (mineral symbol – Hfk), the first Sc-dominant member of the epidote supergroup (IMA2022-139, Pieczka *et al.*, 2023). Crystals with Sc_2O_3 contents lower than ~4.5–5.0 wt.% represent Sc-rich allanite-(Ce) or Sc-rich clinozoisite. Similar mineralisation, with Sc-bearing members of the epidote–allanite-(Ce) solid-solution series locally evolving to heflikite, is known from the Heftetjern pegmatite, Telemark, Norway (samples of Roy Kristiansen) that is a cotype locality for the mineral (Raade and Kristiansen, 2000; Kristiansen, 2009). The purpose of this paper is to report the characteristics of the new mineral heflikite.

Heflikite is isostructural with monoclinic epidote-supergroup minerals and is related to clinozoisite, $Ca_2(^{M1}Al^{M2}Al^{M3}Al)(Si_2O_7)(SiO_4)O(OH)$, and epidote, $Ca_2(^{M1}Al^{M2}Al^{M3}Fe^{3+})(Si_2O_7)(SiO_4)O(OH)$, by isovalent substitutions $^{M3}Sc^{3+} \rightarrow {}^{M3}Al$ and $^{M3}Sc^{3+} \rightarrow {}^{M3}Fe^{3+}$, respectively. In the classification of Strunz and Nickel (2001), the mineral belongs to subgroup 9.BG. Sorosilicates with mixed SiO_4 and Si_2O_7 groups; cations in octahedral and greater coordination. In the classification of Dana (Gaines *et al.*, 1997), it belongs to class 52.2.1a Nesosilicates: Insular, mixed, single, and larger tetrahedral groups with cations in [6] and higher coordination; single and double groups ($n = 1, 2$). The name of the mineral honours Wiesław Heflik (born in 1932), an Emeritus Professor at the Faculty of Geology, Geophysics, and Environmental Protection, AGH University in Kraków, Poland, for his significant contribution to Polish mineralogy, gemology and petrology. He is one of the founding members of the Mineralogical Society of Poland and the Polish Gemological Society. Wiesław Heflik was also the first researcher to study in detail mineral parageneses of the Jordanów Śląski leucocratic rocks.

Holotype heflikite (specimen J11 from Jordanów Śląski) is deposited in the Mineralogical Museum at the University of Wrocław, with the catalogue number MMUWr IV8120. The postal address of the museum is as follows: University of Wrocław, Faculty of Earth Science and Environmental Management, Institute of Geological Sciences, Mineralogical Museum, Cybulskiego 30, 50-205 Wrocław, Poland. The cotype specimen (specimen N5, Heftetjern pegmatite, Tørdal, Telemark, Norway) is deposited in the Natural History Museum, University of Oslo, Norway, with the catalogue number KNR 44407.

Occurrence

Heflikite was discovered in a granitic pegmatite from a serpentinite quarry situated ~1 km west of the Jordanów Śląski village, ~30 km south of Wrocław, Lower Silesia, SW Poland (50.87111°N, 16.83833°E). The quarry is located in the eastern part of the Gogołów-Jordanów Serpentinite Massif, an ultramafic member of the Variscan Ślęża Ophiolite, at the northeastern periphery of the Bohemian Massif in the European Variscides. The Ślęża Ophiolite is a part of the ~400 Ma assemblage of Central Sudetic ophiolites formed in a supra-subduction setting during the amalgamation of Pangea (e.g. Pin *et al.*, 1988; Dubińska *et al.*, 2004; Kryza and Pin, 2010; Awdankiewicz *et al.*, 2021; Wojtulek *et al.*, 2021). Together with the mafic members of the Ślęża Ophiolite exposed to the north and north-west, the serpentinites were subjected to regional greenschist- to lower amphibolite-facies metamorphism.

Small-sized dykes of plagiogranitic appearance and bodies of rodingite-like calc-silicate rocks are distributed randomly in the Gogołów–Jordanów Serpentinite Massif. The latter occur usually as tectonic inclusions in sheared and sometimes also brecciated serpentinites and represent two genetic groups, i.e. boninitic and plagiogranitic rodingites (Dubińska, 1995, 1997). In the Jordanów Śląski quarry, the serpentinites, built mostly of antigorite with minor chrysotile (Dubińska and Szafranek, 1990; Gil *et al.*, 2015, 2020, and references therein), host two roughly NE–SW trending steeply dipping bodies of calc-silicate rocks: one ~20–25 m, the other ~5 m wide, traditionally called 'leucocratic zones'. These rocks show diverse mineralogy dominated by grossular-rich garnet, zoisite and/or clinozoisite, epidote, prehnite and diopside, among others, and are believed to have formed from plagiogranitic-type protolith (e.g. Heflik, 1967, 1982; Majerowicz, 1984; Dubińska and Szafranek, 1990; Dubińska, 1995, 1997). Both rodingitic bodies are surrounded by discontinuous and tectonically disrupted 'blackwall schists', from a few cm to ~1 m thick, containing mostly chlorite, vermiculite, tremolite, and locally also talc (Dubińska and Wiewióra, 1988; Dubińska and Szafranek, 1990). In places, the blackwall schists grade into nephritic rocks composed of antigorite, tremolite and chlorite, with minor actinolite and diopside (Gil, 2013; Gil *et al.*, 2015, 2020). The rodingitic bodies also host strongly metasomatised leucogranite dated at ~340 Ma (Kryza, 2011) and subordinate aplite–pegmatite of an unknown age. The leucogranite is built predominantly of quartz, albite and K-feldspar, with broadly varying minor contents of grossular-rich garnet, actinolite, chlorite, zoisite and/or clinozoisite, diopside and accessory apatite (Kryza, 2011). The pegmatite occurs within fine-grained aplitic rocks as irregular segregations and veins, typically from several centimetres to a little more than 10 cm thick (Waleńczak, 1969; Lis and Sylwestrzak, 1981). The relation of the aplite–pegmatite to the leucogranite remains ambiguous. Lis and Sylwestrzak (1981) described the pegmatite as composed mostly of quartz, feldspars and muscovite, with minor to accessory beryl, almandine–spessartine garnet, tourmaline, unspecified columbite-group minerals, and gahnite. The emplacement of the leucogranite and aplite–pegmatite resulted in both thermal and metasomatic alterations of the surrounding rodingites and serpentinites (Dubińska, 1995; Kryza, 2011). Locally, all the rocks building the 'leucocratic zones' as well as the adjacent serpentinites were mylonitised or brecciated, or both, and cemented by hydrothermal quartz (Dubińska, 1995).

Because the quarry has not been operating for the last 50 years the present state of the exposure is poor and the pegmatite is no longer observed in the quarry walls. Therefore, our investigations have been carried out on samples collected in the 1990s by A.P. Pegmatitic fragments at our disposal are represented by an undeformed and coarse-grained rock, locally with quartz–feldspar graphic texture and weak to moderate overprint of Ca-metasomatic alteration. The pegmatite consists mainly of quartz, sodic plagioclase and K-feldspar, with accessory pale green beryl, dark green dravite, and randomly scattered aggregates of greenish yellow clinochlore. Detailed investigations also revealed the presence of biotite, muscovite, spessartine, titanite, zircon, cassiterite, columbite-(Mn), fersmite, euxenite-(Y), monazite-(Ce), xenotime-(Y), allanite-(Ce), epidote, clinozoisite, rhabdophane-(La),

rhabdophane-(Ce), rhabdophane-(Nd), pyrochlore- and microlite-group minerals, phenakite, bavenite, bertrandite, milarite, tremolite, diopside, uraninite, aikinite, galena, Sc-rich ixiolite and a few Sc-bearing silicates, including cascandite, Sc-rich actinolite (Pieczka *et al.*, 2024a), scandio-winchite (Pieczka *et al.*, 2024b), kristiansenite, bazzite and heflikite (Pieczka *et al.*, 2023).

The sample with cotype heflikite (provided by R.K.) comes from the Heftetjern pegmatite, Tørdal region, Telemark, Norway, the locality widely known for Sc mineralisation hosted in a granitic pegmatite of the Late-Proterozoic Sveconorwegian Pegmatite Province. The Sveconorwegian orogen (1.1–0.9 G.a.) hosts one of the largest pegmatitic provinces in the world, with more than 5000 pegmatite bodies divided into several pegmatite fields (Rosing-Schow *et al.*, 2019). Pegmatites of the Tørdal area in Telemark are situated within the Nissedal volcano-sedimentary outlier. Both the outlier (1.3–1.2 G.a.) and the older basement (1.52–1.50 G.a.) are intruded by the Tørdal granite (960–850 M.a.), regarded as the source of the pegmatite-forming melts (Bergstøl and Juve, 1988). The Tørdal area pegmatites differ geochemically from pegmatites of other districts in southern Norway by having relatively high concentrations of Sn, Sc, Be and Li. On the basis of trace-element analyses of different rock types, it has been suggested that some Sn and a major part of Sc in the Tørdal pegmatites probably had their source in the volcanogenic rocks of the Nissedal outlier, which were penetrated by the F-bearing pegmatitic fluids (Bergstøl and Juve, 1988).

The Heftetjern pegmatites were exposed for the first time by small-scale blasting performed by the land-owner in the early 1970s. This mining activity was mainly aimed at prospecting for good-quality amazonite, which had been quarried by him since the early 1940s in the amazonite–lepidolite pegmatite in the nearby Høydalen quarry. The Heftetjern cleavelandite–amazonite pegmatite is situated in a marshy land between Høydalen and Skarsfjell in Tørdal, southern Norway (59.18223°N, 8.74668°E), ~4.8 km northwest of the small parish of Tørdal. The mineralogy of this pegmatite and the general geology of the area were first described by Bergstøl and Juve (1988), who reported on an unusual occurrence of Sc-rich ixiolite, Sc-rich members of the pyrochlore and microlite groups, and Cs-rich bazzite. The Heftetjern pegmatite is a dyke, ~300 m long and 5 to 40 m thick, hosting a zone, less than 10 m long, 3–4 m wide and less than 2 m deep, extremely enriched in Sc and Be minerals (Kristiansen, 2009). The pegmatite is weakly zoned and consists dominantly of amazonitic microcline, albite (including the cleavelandite variety) with minor oligoclase, quartz (partly smoky), and a variety of dark and white micas. The main accessory minerals are beryl, spessartine, allanite-(Ce), uedaite-(Ce), gadolinite-(Y), cassiterite, Sc-rich ixiolite, zircon, monazite-(Ce), Sc-bearing pyrochlore-supergroup minerals, milarite and phenakite. A late-stage mineral assemblage, present mainly in vugs and fractures, comprises agakhanovite-(Y), bazzite, bertrandite, bohseite, cascandite, Ce–La–Sc-enriched epidote–allanite minerals, Y-rich fluorite, heftetjernite, Mn-bearing hellandite-(Y), Sc-rich helvine, triclinic Ca-hingganite-(Y), Sc-rich garnet, oftedalite, rynersonite, scandiobabingtonite, thortveitite, triclinic titanite and the unnamed new species of OH-dominant analogue of gadolinite-(Y), $(Y,Ca)_2(Fe,\square)Be_2Si_2O_8(OH,O)_2$ (Raade and Erambert, 1999; Raade and Bernhard, 2003; Raade and Kristiansen, 2003; Raade *et al.*, 2002, 2004; Cooper *et al.*, 2006, 2019; Lussier *et al.*, 2009; Kolitsch *et al.*, 2010; Hawthorne *et al.*, 2014; Miyawaki *et al.*, 2015; Chukanov *et al.*, 2017; Raade, 2020; Steffenssen *et al.*, 2020). Heflikite is a part of this late-stage mineral assemblage. The occurrence of well-formed epidote–allanite crystals enriched in Sc (from 2 to 5 wt.% Sc_2O_3) was first documented by reconnaissance scanning electron microscopy (SEM) using energy dispersive spectroscopy (EDS) analyses carried out in 1999. Subsequent detailed electron probe micro-analyses (EPMA) showed that the crystals are chemically zoned with considerable variation in Sc content, locally exceeding 8 wt.% Sc_2O_3 (pers. comm. to R.K. from Dr M. Nagashima, Yamaguchi University, 2017; Kristiansen, 2018).

Appearance and physical properties

At Jordanów Śląski, heflikite was found in the form of a few compositionally zoned euhedral to subhedral separate crystals and intergrowths with REE-bearing clinozoisite and allanite-(Ce), reaching a maximum of 100 μm in size (Figs 1, 2). Textural observations indicate that the crystallisation sequence starts with heflikite (core or inner zone of the aggregates), progresses to Sc-rich allanite-(Ce), Sc-rich clinozoisite and finally to clinozoisite. In the Heftetjern pegmatite, heflikite occurs as a late-stage crystallisation phase in vugs and miarolitic cavities within feldspar and quartz, and is associated with Sc-rich allanite-(Ce), rarely with allanite-(La) and hingganite-(Y). The epidote-supergroup minerals from the locality form grey, green and brown well-developed transparent crystals and fan- or sheaf-like polycrystalline aggregates up to 10 mm large (Fig. 3). Although appearing homogeneous to the naked eye, all crystals examined show complex compositional zoning under SEM-EDS examination, reaching the heflikite composition only in some small domains (Fig. 1g,h).

Heflikite has a white streak, vitreous lustre and a Mohs hardness of ~6 by analogy with other epidote-supergroup minerals. Cleavage, parting, tenacity, fracture and magnetic properties were not observed. Density was not measured owing to the extremely small amount of the mineral. The density calculated from the empirical formula and refined unit-cell volume of the holotype is 3.537 $g \cdot cm^{-3}$. The optical properties were not measured owing to the scarcity of the type material. Heflikite is biaxial, with a mean refractive index close to 1.727, the value calculated from the Gladstone–Dale relation (Mandarino 1979, 1981) using the empirical EPMA-derived formula and calculated density of the holotype crystal.

Chemical composition

Crystals of heflikite were analysed at the Inter-Institute Analytical Complex for Minerals and Synthetic Substances at the University of Warsaw, Poland, using a Cameca SX 100 electron microprobe operating in wavelength-dispersive X-ray spectrometry mode (WDS) with an accelerating voltage of 15 kV, a beam current of 20 nA, peak count-time of 20 s, background time of 10 s, and a beam diameter of 2 μm. The microprobe is equipped with five spectrometers with the following diffracting crystals: TAP (thallium acid phthalate), PET (pentaerythritol), LIF (lithium fluoride), LPET (pentaerythritol – large crystal), LLIF (lithium fluoride – large crystal), and PC0 (W/Si multilayer crystal). Four analyses have been made on the holotype and three on the cotype. Reference materials, diffracting crystals, analytical lines and mean detection limits (element, wt.%) were as follows: F (fluorophlogopite, PC0, *K*α, 0.12), Mg (diopside, TAP, *K*α, 0.02), Al (orthoclase, TAP, *K*α, 0.02), Si (diopside, TAP, *K*α, 0.02), Ca (diopside, PET, *K*α, 0.03), Sc (pure Sc, *K*α, PET,

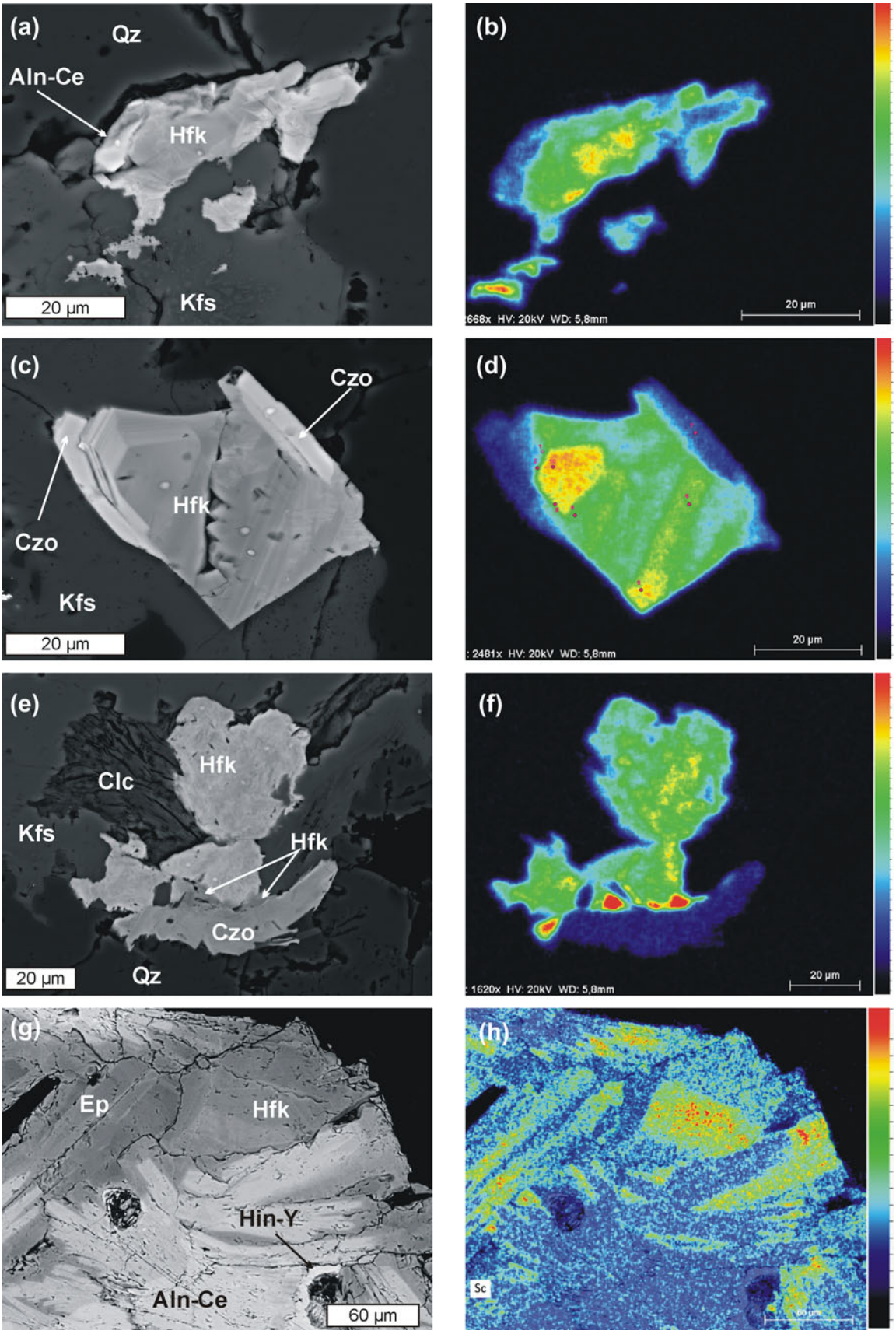

Figure 1. Back-scattered electron (BSE) images and Sc distribution maps of heflikite crystals in the holotype (J11) and cotype (N5) specimens: (a,b) the studied holotype crystal J11a; (c,d) heflikite J11c evolving to Sc-rich clinozoisite; (e,f) heflikite J11b intergrown with Sc-poor clinozoisite; (g,h) an aggregate of allanite-(Ce) from the Heftetjern pegmatite with domains of heflikite (N5). Abbreviations: Aln-Ce – allanite-(Ce), Clc – clinochlore, Czo – clinozoisite, Ep – epidote, Hin-Y – hingganite-(Y), Kfs – K-feldspar, Qz – quartz (Warr, 2021), Hfk – heflikite.

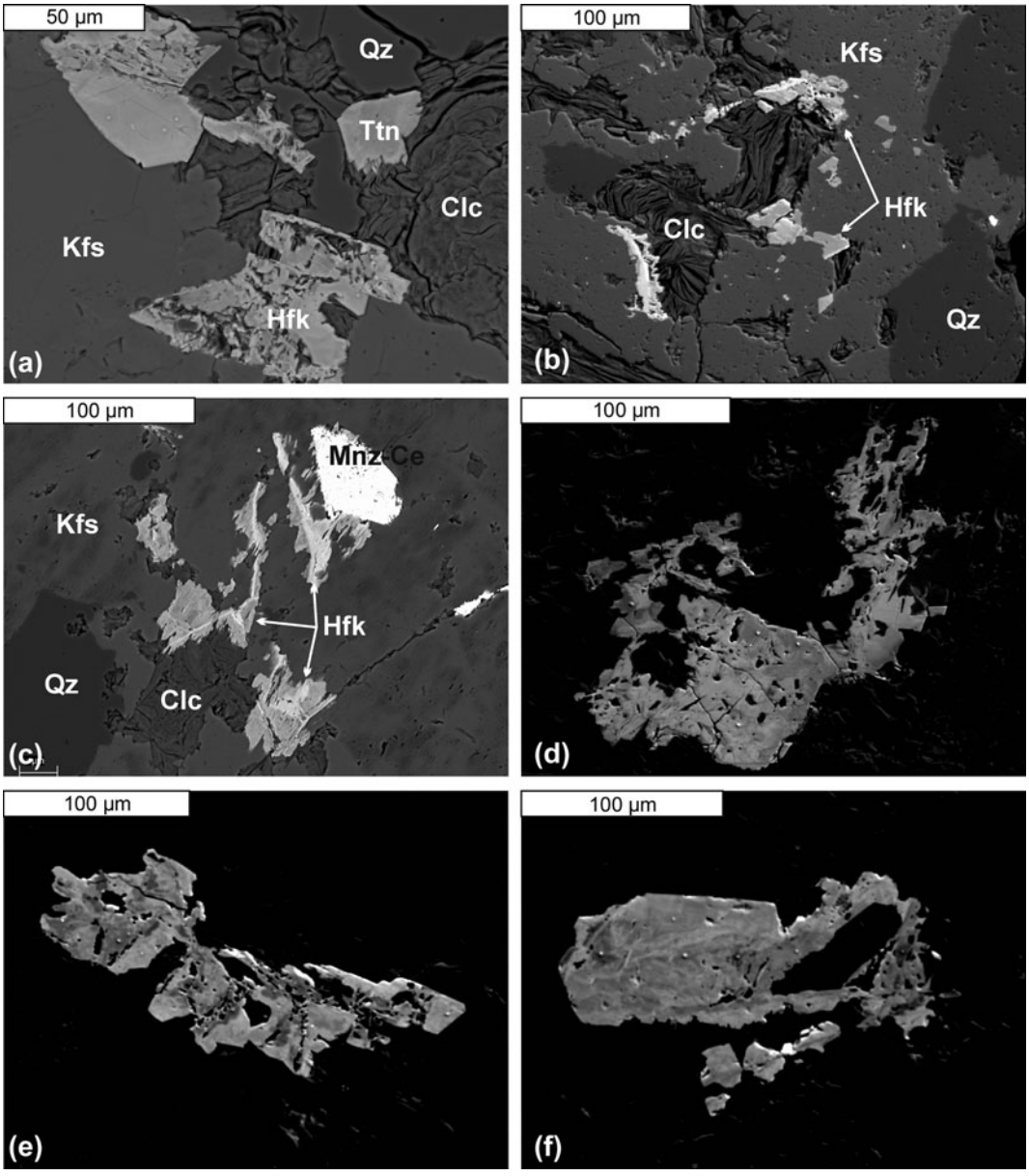

Figure 2. BSE images of other heflikite–allanite-(Ce) aggregates in specimens J15, J18, J19b (a–c) and J20c (d–f) from Jordanów. Abbreviations: Mnz-Ce – monazite-(Ce), Ttn – titanite, others as in Fig. 1. Darker zones in Figs 2d–f correspond to heflikite and lighter ones to Sc-rich allanite-(Ce) or Sc-rich REE-bearing clinozoisite.

0.02), Ti (rutile, *K*α, PET, 0.03), V (V_2O_5, *K*α, LIF, 0.07), Cr (chromite, *K*α, LIF, 0.07), Mn (rhodonite, *K*α, LIF, 0.06), Fe (hematite, *K*α, LIF, 0.06), Zn (sphalerite, *K*α, LIF, 0.08), Sr (celestine, *L*α, TAP, 0.06), Y (YPO_4, *L*α, TAP, 0.04), Sn (cassiterite, PET, *L*α, 0.07), La ($LaPO_4$, *L*α, PET, 0.08), Ce ($CePO_4$, *L*α, PET, 0.07), Pr (Pr glass, *L*β, LIF, 0.14), Nd ($NdGaO_3$, *L*β, LLIF, 0.12), Sm ($SmPO_4$, *L*β, LLIF, 0.13), Eu ($EuPO_4$, *L*α, LLIF, 0.05), Gd ($GdPO_4$, *L*α, LLIF, 0.06), Tb ($TbPO_4$, *L*α, LLIF, 0.08), Dy ($DyPO_4$, *L*α, LLIF, 0.07), Er ($ErPO_4$, *L*α, LLIF, 0.08), Ho ($HoPO_4$, *L*β, LLIF, 0.18), Tm ($TmPO_4$, *L*α, LLIF, 0.07), Yb ($YbPO_4$, *L*α, LLIF, 0.09), Lu ($LuPO_4$, *L*β, LLIF, 0.16), Pb (crocoite, *M*α, PET, 0.15), Th (ThO_2, *M*α, PET, 0.15) and U (UO_2, *M*β, PET, 0.15). The raw data were reduced with the 'PAP' routine of Pouchou and Pichoir (1991). The problem of the analytical-line interferences for lanthanides has been addressed following the recommendations of Reed and Buckley (1998). The content of H_2O was not measured owing to the scarcity of the material. It was calculated from the empirical formula, assuming 1 OH anion per formula unit on the basis of the generalised formula of the epidote-supergroup minerals. The empirical formula was normalised to 12 O atoms + 1 (OH) group, with a Fe^{3+}/Fe_{total} ratio matched in such a way to obtain the total content of all cations equal to 8 per formula unit. Compositional data of the holotype and cotype crystals are given in Table 1. On the basis of the general formula of the epidote-supergroup minerals, $A_2M_3[T_2O_7][TO_4](O,F)(OH,O)$, and suggested assignments of cations to different structural sites (Armbruster *et al.*, 2006), the averaged compositions correspond to the following empirical formula for the holotype heflikite from Jordanów Śląski (J11a crystal, Fig. 1a,b):

Figure 3. Crystals of allanite-(Ce)–heflikite solid solution from the Heftetjern pegmatite (Field of view: ~5 × 3 mm). Photo used with permission, copyright Mr. O.T. Ljøstad.

$$^{A1}Ca^{A2}(Ca_{0.729}Ce_{0.125}La_{0.048}Nd_{0.046}Gd_{0.016}Sm_{0.012}Pr_{0.010}Y_{0.005}Eu^{2+}_{0.003})_{\Sigma 0.994}\ ^{M1}Al^{M2}Al^{M3}[(Sc_{0.449}Al_{0.182}Fe^{3+}_{0.070}V^{3+}_{0.005})_{\Sigma 0.706}(Fe^{2+}_{0.251}Mg_{0.020}Mn_{0.010})_{\Sigma 0.281}\ Ti_{0.014}]_{\Sigma 1.001}(Si_{3.006}O_{11})O(OH),$$

and for the cotype heflikite from the Heftetjern pegmatite (Sc-rich domain in N5 specimen, Fig. 1g,h):

$$^{A1}Ca^{A2}(Ca_{0.644}Ce_{0.235}La_{0.082}Nd_{0.021}Gd_{0.018}Pr_{0.015}Eu^{2+}_{0.004})_{\Sigma 1.019}\ ^{M1}(Al_{0.958}Ti_{0.029})_{\Sigma 0.987}\ ^{M2}Al^{M3}[(Sc_{0.362}Fe^{3+}_{0.128})_{\Sigma 0.490}(Fe^{2+}_{0.434}Mn_{0.009})_{\Sigma 0.443}\ Sn_{0.029}]_{\Sigma 0.962}(Si_{3.033}O_{11})O(OH).$$

The empirical formula of the holotype corresponds to the simplified heflikite formula $Ca(Ca,Ce)Al_2(Sc,Al,Fe^{3+},Fe^{2+})(Si_2O_7)(SiO_4)O(OH)$, and the ideal formula $Ca_2(Al_2Sc)(Si_2O_7)(SiO_4)O(OH)$, which requires (in wt.%) SiO_2 38.16, Al_2O_3 21.59, Sc_2O_3 14.60, CaO 23.74, and H_2O 1.91; Total 100. The crystal from the Heftetjern pegmatite represents an intermediate member in a solid solution with allanite-type species. It shows a small prevalence of the heflikite end-member over allanite, but this is strongly dependent on the position of Ti^{4+} in the structure (M1 or M3 site). Supplementary material (S1), deposited with the Principal Editors of *Mineralogical Magazine*, presents the chemical compositions of the most Sc-rich heflikite domains in other heflikite – clinozoisite – Sc-rich allanite-(Ce) intergrowths from the Jordanów Śląski pegmatite (Figs 1 and 2).

Crystallography

Single-crystal X-ray diffraction and structure refinement

Two single crystals, the holotype J11a and the cotype N5, (0.033 × 0.015 × 0.004 mm and 0.068 × 0.037 × 0.023 mm, respectively), were extracted in the Laboratory of Transmission Electron Microscopy, Academic Centre for Materials and Nanotechnology (AGH University of Krakow), using a Quanta 3D 200i (Thermo Fisher Scientific) scanning electron microscope equipped with a Ga^+ ion gun, Pt precursor gas injection systems (GIS) and Omniprobe micromanipulator for *in situ* lift-out. An ion beam accelerating voltage of 30 kV and ion currents in the range of 60 nA to 1 nA were applied. The sample was transferred *via* a micromanipulator to standard TEM copper half-ring grids. A FIB deposition process (from Pt precursor) was used to attach the manipulator probe to the sample and the foil to the grid. Afterwards, the crystal was transferred to a suitable microloop and placed on the goniometer base. The holotype crystal was attached to a non-diffracting Mitegen micromount support. The cotype crystal was attached to a carbon fibre that was attached to a metal pin.

Single-crystal X-ray diffraction (XRD) measurements were carried out with a four-circle diffractometer SuperNova, equipped with a HyPix (Rigaku Oxford Diffraction) Hybrid Pixel Array Detector. The detector-to-crystal distance was 55.0 mm. We

Table 1. Compositions of heflikite from Jordanów Śląski, Poland, and Heftetjern, Norway (in wt.%, rounded to the second decimal place).

	Jordanów Śląski (holotype J11a; *n* = 4)					Heftetjern (cotype N5; *n* = 3)					
Constituent	Mean	Range	σ		apfu	Mean	Range	σ		apfu	Reference material
SiO_2	35.69	35.46–35.93	0.20	Si^{4+}	3.006	34.92	33.94–35.53	0.60	Si^{4+}	3.033	diopside
TiO_2	0.22	0.13–0.29	0.07	Ti^{4+}	0.014	0.44	0.35–0.67	0.13	Ti^{4+}	0.029	rutile
SnO_2	b.d.l.	b.d.l.		Sn^{4+}		0.82	0.64–0.96	0.13	Sn^{4+}	0.029	cassiterite
Al_2O_3	21.98	21.48–22.48	0.44	Al^{3+}	2.182	19.13	17.83–20.12	0.97	Al^{3+}	1.958	orthoclase
Sc_2O_3	6.12	5.06–7.22	0.93	Sc^{3+}	0.449	4.79	4.14–5.32	0.52	Sc^{3+}	0.362	Sc
V_2O_3	0.07	0.05–0.09	0.02	V^{3+}	0.005	b.d.l.	b.d.l.		V^{3+}		V_2O_5
Fe_2O_3 [a)]	1.10	0.51–1.88		Fe^{3+}	0.070	1.96	0.29–2.65		Fe^{3+}	0.128	
Y_2O_3	0.11	b.d.l.–0.27	0.12	Y^{3+}	0.005	b.d.l.	b.d.l.		Y^{3+}		YPO_4
La_2O_3	1.55	1.46–1.62	0.08	La^{3+}	0.048	2.55	1.98–3.95	0.79	La^{3+}	0.082	$LaPO_4$
Ce_2O_3	4.05	3.97–4.14	0.07	Ce^{3+}	0.125	7.39	6.58–8.85	0.86	Ce^{3+}	0.235	$CePO_4$
Pr_2O_3	0.31	0.21–0.38	0.08	Pr^{3+}	0.010	0.48	0.22–0.59	0.16	Pr^{3+}	0.015	Pr glass
Nd_2O_3	1.53	1.38–1.62	0.10	Nd^{3+}	0.046	0.67	0.52–0.81	0.12	Nd^{3+}	0.021	$NdGaO_3$
Sm_2O_3	0.40	0.21–0.54	0.14	Sm^{3+}	0.012	b.d.l.	b.d.l.		Sm^{3+}	0.000	$SmPO_4$
EuO	0.11	0.09–0.13	0.02	Eu^{2+}	0.003	0.12	0.05–0.16	0.05	Eu^{2+}	0.004	$EuPO_4$
Gd_2O_3	0.56	0.54–0.58	0.02	Gd^{3+}	0.016	0.61	0.52–0.73	0.09	Gd^{3+}	0.018	$GdPO_4$
MnO	0.14	0.08–0.19	0.05	Mn^{2+}	0.010	0.13	0.08–0.22	0.06	Mn^{2+}	0.009	rhodonite
FeO [a)]	3.56	3.30–3.83		Fe^{2+}	0.251	5.97	5.23–7.66		Fe^{2+}	0.434	hematite
MgO	0.16	0.12–0.20	0.04	Mg^{2+}	0.020	b.d.l.	b.d.l.		Mg^{2+}		diopside
CaO	19.16	18.87–19.49	0.27	Ca^{2+}	1.729	17.66	15.86–18.51	1.05	Ca^{2+}	1.644	diopside
$H_2O^{(+)}_{calc.}$	1.78	1.77–1.79		OH^-	1.000	1.73	1.67–1.76		OH^-	1.000	
Total	98.60					99.37					

Notes: *n* – number of spot analyses; σ – standard deviation; b.d.l. – below detection limit; [a)] total Fe measured as FeO in the Jordanów Śląski heflikite was equal to 4.55 wt.% (range: 3.76–5.32 wt.%; σ: 0.77 wt.%) and 7.73 wt.% in the Heftetjern heflikite (range: 7.44–7.93 wt.%; σ: 0.22 wt.%). The Fe_2O_3 and FeO contents were calculated on the basis of the stoichiometry of the epidote-supergroup minerals. Terbium, Dy, Ho, Er, Tm, Yb, Lu, Th, U, Cr, Sr, Zn, Pb and F were below the respective detection limits (b.d.l.); $H_2O_{calc.}$ – calculated on the basis of OH = 1 anion pfu.

used Cu*K*α radiation (λ = 1.54184 Å) at 50.00 kV and 0.80 mA. A frame width of 1° in ω scans and frame times of 7, 30 and 50 s for holotype (2, 8 and 20 s for cotype) were used in the data collection strategy. Reflection intensities were corrected for Lorentz, polarisation, and absorption effects and converted to structure factors using the *CrysAlisPro* 1.171.42.36a software (Rigaku Oxford Diffraction, 2021). The holotype and cotype samples, although forming aggregates, enabled the separation of their components and facilitated single crystal processing.

The anisotropic structure refinement was performed in the space group $P2_1/m$ using *Shelxl* (Sheldrick, 2015), within the *Olex2* (Dolomanov *et al.*, 2009) graphical interface, starting from the atomic coordinates of Dollase (1969). Correct element-assignment for cations and anions was based upon compositional data obtained by EPMA and crystal-chemical reasoning following the suggestions by Armbruster *et al.* (2006), comprising site-scattering, coordination and bond-lengths. The hydrogen atom position was found from the difference-Fourier maps of residual electron density. Final positions of H atoms were determined from the least-squares refinement with a restraint of bond length equal to 0.97(1) Å. This value is determined from a neutron diffraction experiment, which more accurately determines the H atom position (Gatta *et al.*, 2010).

The structure was refined with the least-squares minimisation to $R_1 = 8.62\%$ (holotype) and 6.37% (cotype). Elevated values of R_1 indices are caused by compositional heterogeneity and moderate crystallinity of the extracted crystals (see Fig. 1a,b and g,h). Where more than one element occupied the same position in the asymmetric unit, constraints for equal atom coordinates and equal anisotropic displacement parameters for these groups of atoms within each unique site were applied.

Compositions of the refined crystals and initial refinements indicated that the A1 site is occupied solely by Ca, the M1 site (in holotype) and M2 site by Al, and the T1–T3 sites by Si. Therefore, the corresponding site occupancies were fixed as the respective full atom in the final refinement. Regarding the cotype heflikite, the M1 site occupancy was set free for refinement with the Al scattering factor. The occupancies of M3 and A2 sites were constrained to 1 and refined as ^{M3}(Sc *vs* Al) for holotype, ^{M3}(Sc *vs* Fe) for cotype, and ^{A2}(Ca *vs* Ce) for both crystals. Details of the measurements and structure solutions are presented in Table 2. Refined atom positions, equivalent isotropic and anisotropic displacement parameters, and occupancy for structural sites are given in Table 3, selected bond-lengths are collected in Table 4, and assigned site-populations are shown in Table 5. Bond-valences calculated on the basis of the parameters given by Gagné and Hawthorne (2015) are shown in Table 6. A comparison of the epidote-group minerals, including heflikite, is presented in Table 7. The crystallographic information file has been deposited with the Principal Editor of *Mineralogical Magazine* and is available as Supplementary material (S2).

Crystal structure

Heflikite crystallises in the monoclinic system ($P2_1/m$ space-group symmetry), with unit-cell parameters (for holotype):

Table 2. Details on data collection and structure refinement of heflikite.

	J11a	N5
Crystal data		
Crystal size	0.033 × 0.015 × 0.004 mm	0.068 × 0.037 × 0.023 mm
Crystal system	monoclinic	monoclinic
Space group	$P2_1/m$	$P2_1/m$
Unit-cell dimensions	a = 8.9383(9) Å	a = 8.9232(6) Å
	b = 5.6830(5) Å	b = 5.6746(3) Å
	c = 10.1903(10) Å	c = 10.1626(9) Å
	β = 115.043(12)°	β = 115.001(10)°
Unit-cell volume	468.97(9) Å^3	466.38(7) Å^3
Z	2	2
Calculated density	3.537 g·cm^{-3}	3.652 g·cm^{-3}
Data collection and refinement		
Instrument	SuperNova, Dual, Cu, Hypix (Rigaku – Oxford Diffraction) four circle diffractometer with a mirror monochromator	SuperNova, Dual, Cu, Hypix (Rigaku – Oxford Diffraction) four circle diffractometer with a mirror monochromator
X-ray radiation source	Cu*K*α (λ = 1.54184 Å)	Cu*K*α (λ = 1.54184 Å)
Temperature	287 K	297 K
Absorption coefficient	31.78 mm^{-1}	37.69 mm^{-1}
F(000)	490	499
θ range for data collection	θ_{max} = 77.4°, θ_{min} = 4.8°	θ_{max} = 77.1°, θ_{min} = 4.8°
θ full	67.6°	76.6°
Index ranges	$-11 \le h \le 11$, $-7 \le k \le 5$, $-12 \le l \le 12$	$-11 \le h \le 11$, $-7 \le k \le 7$, $-12 \le l \le 12$
Reflections collected	4984	11526
Independent reflections	1083 [R_{int} = 0.094]	1067 [R_{int} = 0.098]
Reflections with $I_o > 2\sigma I$	958	1017
Completeness to θ_{max}	98.3%	97.6%
Completeness to θ full	100%	97.7%
Refinement method	Full-matrix least-squares on F^2	Full-matrix least-squares on F^2
Parameters / restraints	124/3	124/3
Goodness-of-fit on F^2	1.22	1.17
Final R indices [$I_o > 2\sigma(I)$]	R_1 = 0.0862 wR_2 = 0.214	R_1 = 0.0637 wR_2 = 0.17
Largest diff. peak and hole in e^-/Å^3	+1.55 (0.97 Å from A2 site)	1.77 (1.01 Å from A2 site)
	−1.41 (0.79 Å from O7)	−1.17 (0.95 Å from M3 site)

*$R_{int} = \Sigma|F_o^2 - F_{o(mean)}^2|/\Sigma[F_o^2]$. GooF = $S = \{\Sigma[w(F_o^2 - F_c^2)^2]/(n-p+r)\}^{1/2}$. $R_1 = \Sigma||F_o| - |F_c||/\Sigma|F_o|$. $wR_2 = \{\Sigma[w(F_o^2 - F_c^2)^2]/\Sigma[w(F_o^2)^2]\}^{1/2}$; $w = 1/[\Sigma^2(F_o^2) + (aP)^2 + bP]$, where a is 0.103^{J11a}, 0.0991^{N5} b is 4.1644^{J11a}, 2.5299^{N5} and P is $[2F_c^2 + F_o^2)]/3$.

Table 3. Atomic coordinates, occupancy, equivalent/isotropic and anisotropic displacement parameters (Å^2) for non-hydrogen atoms for heflikite.

Site	Atom	Occupancy	*x/a*	*y/b*	*z/c*	U_{eq}/U_{iso}*	U^{11}	U^{22}	U^{33}	U^{23}	U^{13}	U^{12}
Jordanów Śląski (holotype J11a)												
A1	Ca	1	0.7599(4)	¾	0.1521(3)	0.0259(8)	0.0306(17)	0.0255(16)	0.0247(15)	0	0.0147(13)	0
A2	Ca,Ce	$Ca_{0.698(8)}Ce_{0.302(8)}$	0.5989(2)	¾	0.42561(18)	0.0289(7)	0.0275(11)	0.0336(12)	0.0202(10)	0	0.0046(8)	0
M1	Al	1	0	0	0	0.0244(10)	0.023(2)	0.025(2)	0.024(2)	0.0006(18)	0.0087(17)	0.0009(19)
M2	Al	1	0	0	½	0.0216(9)	0.022(2)	0.020(2)	0.0195(19)	0.0016(17)	0.0059(16)	0.0015(18)
M3	Sc,Al	$Sc_{0.83(4)}Al_{0.17(4)}$	0.2982(4)	¼	0.2183(3)	0.0235(10)	0.0199(16)	0.0257(18)	0.0201(16)	0	0.0037(12)	0
T1	Si	1	0.3384(5)	¾	0.0426(4)	0.0232(9)	0.021(2)	0.028(2)	0.0200(19)	0	0.0073(16)	0
T2	Si	1	0.6872(5)	¼	0.2759(4)	0.0240(9)	0.027(2)	0.025(2)	0.0191(19)	0	0.0093(17)	0
T3	Si	1	0.1859(5)	¾	0.3204(4)	0.0192(9)	0.0176(18)	0.024(2)	0.0148(17)	0	0.0060(14)	0
O1	O	1	0.2348(9)	0.9912(14)	0.0357(7)	0.0275(17)	0.031(4)	0.028(4)	0.024(4)	0.003(3)	0.012(3)	0.004(3)
O2	O	1	0.3059(8)	0.9789(14)	0.3581(7)	0.0269(17)	0.024(4)	0.035(4)	0.021(3)	−0.006(3)	0.009(3)	−0.008(3)
O3	O	1	0.7973(8)	0.0144(13)	0.3389(8)	0.0265(16)	0.018(3)	0.025(4)	0.027(4)	−0.004(3)	0.001(3)	−0.002(3)
O4	O	1	0.0505(13)	¼	0.1288(10)	0.025(2)	0.026(5)	0.025(6)	0.016(5)	0	0.002(4)	0
O5	O	1	0.0450(12)	¾	0.1478(11)	0.024(2)	0.024(5)	0.023(5)	0.023(5)	0	0.009(4)	0
O6	O	1	0.0684(13)	¾	0.4090(11)	0.026(2)	0.027(6)	0.028(6)	0.025(5)	0	0.013(5)	0
O7	O	1	0.5117(12)	¾	0.1800(10)	0.026(2)	0.020(5)	0.039(6)	0.015(5)	0	0.003(4)	0
O8	O	1	0.5338(16)	¼	0.3195(14)	0.043(3)	0.047(8)	0.053(8)	0.042(7)	0	0.031(6)	0
O9	O	1	0.6250(16)	¼	0.1018(13)	0.040(3)	0.051(8)	0.044(8)	0.031(6)	0	0.023(6)	0
O10	O	1	0.0853(13)	¼	0.4312(9)	0.023(2)	0.031(6)	0.023(5)	0.009(4)	0	0.004(4)	0
H10	H	1	0.084(14)	¼	0.335(5)	0.034*						
Heftetjern (cotype N5)												
A1	Ca	1	0.7607(3)	¾	0.1517(2)	0.0227(5)	0.0361(11)	0.0161(9)	0.0286(11)	0	0.0260(9)	0
A2	Ca,Ce	$Ca_{0.636(6)}Ce_{0.364(6)}$	0.59681(13)	¾	0.42658(12)	0.0246(4)	0.0314(7)	0.0236(6)	0.0264(7)	0	0.0195(5)	0
M1	Al	$Al_{0.940(16)}$	0	0	0	0.0188(10)	0.0255(16)	0.0130(15)	0.0255(18)	−0.0026(11)	0.0183(13)	−0.0001(11)
M2	Al	1	0	0	½	0.0166(6)	0.0244(13)	0.0133(12)	0.0214(14)	−0.0005(10)	0.0187(11)	−0.0005(10)
M3	Sc,Fe	$Sc_{0.48(4)}Fe_{0.52(4)}$	0.2981(2)	¼	0.21761(19)	0.0198(5)	0.0260(9)	0.0182(9)	0.0230(10)	0	0.0177(7)	0
T1	Si	1	0.3400(3)	¾	0.0440(3)	0.0185(6)	0.0275(13)	0.0156(12)	0.0216(13)	0	0.0192(11)	0
T2	Si	1	0.6880(3)	¼	0.2773(3)	0.0181(6)	0.0260(13)	0.0142(12)	0.0223(14)	0	0.0183(11)	0
T3	Si	1	0.1854(3)	¾	0.3202(3)	0.0181(6)	0.0253(12)	0.0146(12)	0.0249(13)	0	0.0209(10)	0
O1	O	1	0.2354(6)	0.9918(9)	0.0373(6)	0.0221(11)	0.030(2)	0.016(2)	0.027(3)	0.0026(18)	0.019(2)	0.0011(19)
O2	O	1	0.3075(6)	0.9776(9)	0.3593(6)	0.0228(11)	0.031(2)	0.021(2)	0.027(3)	−0.002(2)	0.022(2)	−0.004(2)
O3	O	1	0.7971(6)	0.0148(8)	0.3376(6)	0.0221(11)	0.026(2)	0.018(2)	0.028(3)	−0.0019(19)	0.016(2)	−0.0010(19)
O4	O	1	0.0518(8)	¼	0.1296(8)	0.0190(14)	0.027(3)	0.012(3)	0.022(4)	0	0.014(3)	0
O5	O	1	0.0443(9)	¾	0.1483(8)	0.0213(15)	0.035(4)	0.016(3)	0.024(4)	0	0.023(3)	0
O6	O	1	0.0679(8)	¾	0.4093(8)	0.0190(14)	0.025(3)	0.014(3)	0.027(4)	0	0.019(3)	0
O7	O	1	0.5127(9)	¾	0.1789(8)	0.0231(15)	0.034(4)	0.020(3)	0.023(4)	0	0.020(3)	0
O8	O	1	0.5340(9)	¼	0.3208(9)	0.0300(17)	0.029(4)	0.035(4)	0.040(5)	0	0.027(4)	0
O9	O	1	0.6233(10)	¼	0.1015(9)	0.0305(18)	0.042(4)	0.029(4)	0.036(5)	0	0.031(4)	0
O10	O	1	0.0865(8)	¼	0.4308(7)	0.0184(14)	0.027(3)	0.014(3)	0.023(4)	0	0.019(3)	0
H10	H	1	0.054(15)	¼	0.327(3)	0.028*						

* U_{iso} (isotropic displacement parameters).

$a = 8.9383(9)$ Å, $b = 5.6830(5)$ Å, $c = 10.1903(10)$ Å, $\beta = 115.43(12)°$, $V = 468.97(9)$ Å^3; $Z = 2$. The $a : b : c$ ratio calculated from the unit-cell parameters is 1.5728 : 1 : 1.7931.

The crystal structure of the epidote-supergroup minerals, including heflikite, is composed of T_2O_7 (Si_2O_7) and TO_4 (SiO_4) units linked to two kinds of chains built by edge-sharing MO_6 octahedra arranged parallel to the **b** axis (Dollase, 1968, 1969, 1971; Shepel and Karpenko, 1969; Bonazzi *et al.*, 1990; Miyajima *et al.*, 2003; Minakawa *et al.*, 2008; Armbruster *et al.*, 2002, 2006; Chukanov *et al.*, 2012). In heflikite, one chain consists of $^{M2}AlO_5(OH)$ octahedra, while the other is formed by $^{M1}AlO_6$ octahedra with $M3O_6$ octahedra attached on alternate sides along its length (Fig. 4). The $M3O_6$ octahedra are occupied dominantly by trivalent cations (Sc, Al, Fe^{3+} and traces of V^{3+}), from which Sc^{3+} prevails in the holotype. Divalent cations (Fe^{2+}, Mn^{2+} and Mg) are always less abundant in crystals from Jordanów Śląski (Tables 1 and S1) owing to subordinate substitution $^{A2}REE^{3+} + {}^{M3}(Fe,Mn,Mg)^{2+} \leftrightarrow {}^{A2}Ca^{2+} + {}^{M3}(Sc,Al,Fe)^{3+}$. Traces of Ti^{4+} were assigned to the $M3O_6$ octahedron because the M1 site is fully occupied by Al^{3+} in the Jordanów Śląski crystal. In the Heftetjern heflikite, Ti^{4+} was assigned to the M1 site to compensate for Al deficiency [as suggested by Armbruster *et al.* (2006)], while the relatively large Sn^{4+} ion was assigned to the M3 site. The hydroxyl group is bonded to the M2 cation, and the O4 oxygen is not substituted by F.

The EPMA-derived compositions and refined crystal-structure models of the holotype and cotype indicate that tetrahedral T1–T3 sites are fully occupied by Si, corresponding to the typical epidote structure. The two A sites (A1 and A2) in epidote-supergroup minerals can be occupied by Ca and Mn^{2+} at A1, and Ca, Sr, Pb and REE^{3+} with possible subordinate U^{4+}, Th^{4+}, K^+ and Ba^{2+} at A2 (Armbruster *et al.*, 2006). In heflikite, however, Ca contents over 1.5 atoms per formula unit (apfu) suggest that Ca is a dominant occupant also at the A2 site, while REE from La to Gd are subordinate (Tables 1 and S1). The ^{A1}(Ca,Mn) is nine-fold coordinated with (Ca,Mn)–O bond lengths ranging from 2.327(5)–2.335(7) Å to 3.044(5)–3.047(3) Å, with <^{A1}(Ca,Mn)–O> mean distances of 2.603(8) Å and 2.597(5) Å in the holotype and cotype crystals, respectively. The occupation of the A1 site is corroborated by the calculated bond-valence sum (BVS) of 2.01 and 2.05 valence units (vu) in both crystals (Table 6), which closely corresponds to the 2+ valence of Ca and Mn.

The A2 site occupancy was refined as $Ca_{0.698(8)}Ce_{0.302(8)}$ in the holotype and $Ca_{0.636(6)}Ce_{0.364(6)}$ in the cotype (Table 3). The occupancies suggest an A2 site population with 31.6(3) e^- and

Table 4. Selected bond-lengths (Å) and hydrogen bond angle (°) for heflikite.

	Jordanów Śląski (J11c)	Heftetjern (N5)		Jordanów Śląski (J11c)	Heftetjern (N5)		Jordanów Śląski (J11c)	Heftetjern (N5)
^{A1}Ca–O1	2.429(8) ×2	2.428(5) ×2	^{T1}Si–O1	1.639(8) ×2	1.644(5) ×2	O10–H10	0.974(10)	0.968(11)
^{A1}Ca–O3	2.335(7) ×2	2.327(5) ×2	^{T1}Si–O7	1.589(10)	1.571(8)	H10···O2	2.44(9)	2.64(10)
^{A1}Ca–O5	2.567(10)	2.545(7)	^{T1}Si–O9	1.636(12)	1.645(8)	O10···O2	2.839(11)	2.831(7)
^{A1}Ca–O6	2.889(11)	2.881(7)	<^{T1}Si–O>	1.626(9)	1.626(7)			
^{A1}Ca–O7	2.354(10)	2.344(7)	^{T1}<λ>	1.0024	1.0027	O10–H10···O2	104(6)	91(6)
^{A1}Ca–O9	3.044(5) ×2	3.047(3) ×2	^{T1}σ^2	8.4068	8.5881	H10···O4	1.995(10)	2.00(4)
<^{A1}Ca–O>	2.603(8)	2.597(5)				O10···O4	2.963(12)	2.944(10)
			^{T2}Si–O3	1.624(8) ×2	1.613(5) ×2	O10–H10···O4	173(10)	165(11)
A2–O2	2.523(7) ×2	2.506(5) ×2	^{T2}Si–O8	1.610(12)	1.611(7)			
A2–O2	2.738(8) ×2	2.704(5) ×2	^{T2}Si–O9	1.619(12)	1.628(9)			
A2–O3	2.741(7) ×2	2.764(5) ×2	<^{T2}Si–O>	1.619(10)	1.616(7)			
A2–O7	2.285(9)	2.302(7)	^{T2}<λ>	1.0007	1.0009			
A2–O8	3.008(4) ×2	3.002(3) ×2	^{T2}σ^2	2.6073	3.7024			
A2–O10	2.571(10)	2.574(7)						
<A2–O>	2.688(7)	2.683(5)	^{T3}Si–O2	1.626(8) ×2	1.627(5) ×2			
			^{T3}Si–O5	1.674(11)	1.667(8)			
^{M1}Al–O1	1.973(7) ×2	1.971(5) ×2	^{T3}Si–O6	1.650(10)	1.650(7)			
^{M1}Al–O4	1.855(6) ×2	1.857(5) ×2	<^{T3}Si–O>	1.644(9)	1.643(6)			
^{M1}Al–O5	1.984(7) ×2	1.984(5) ×2	^{T3}<λ>	1.0050	1.0060			
<^{M1}Al–O>	1.937(7)	1.937(5)	^{T3}σ^2	19.6744	24.0061			
^{M1}<λ>	1.0057	1.0058						
^{M1}σ^2	13.7482	14.0497	M3–O1	2.248(8) ×2	2.225(5) ×2			
			M3–O2	2.079(8) ×2	2.090(5) ×2			
^{M2}Al–O3	1.862(7) ×2	1.866(5) ×2	M3–O4	2.006(11)	1.992(7)			
^{M2}Al–O6	1.932(6) ×2	1.924(4) ×2	M3–O8	1.913(13)	1.914(8)			
^{M2}Al–O10	1.883(6) ×2	1.887(4) ×2	<M3–O>	2.095(9)	2.089(6)			
<^{M2}Al–O>	1.892(6)	1.892(4)	^{M3}<λ>	1.0309	1.0309			
^{M2}<λ>	1.0054	1.0051	^{M3}σ^2	90.5352	91.9990			
^{M2}σ^2	17.5706	17.1071						

Notes: Quadratic elongation, <λ> and bond variance, σ^2 (degree^2) for octahedra and tetrahedra coordination are as defined by Robinson *et al.* (1971).

33.8(2) e^-, respectively, the values conforming to the numbers of electrons at the site of both refined crystals derived from their empirical formulae, i.e. 30.0(6) e^- and 34.7(2.9) e^-. Considering the moderate quality of the single-crystal XRD data, the final A2 site populations were assigned to those indicated by the empirical EPMA-derived formulae (Table 5). The A2 site occupants are coordinated by 9 oxygen atoms and a hydroxyl from the O10 site, with bond lengths ranging from 2.285(9)–2.302(7) Å to 3.002(3)–3.004(4) Å, and the refined <^{A2}Ca–O> of 2.688(7) Å and 2.683(5) Å. Both in the holotype and cotype, <^{A1}Ca–O> and <A2–O> are slightly larger than 2.59–2.63 Å derived from the empirical compositions on the basis of the effective nine-fold-coordinated Ca^{2+} and ten-fold-coordinated Ca^{2+}, La^{3+},Ce^{3+},Pr^{3+},Nd^{3+},Sm^{3+},Eu^{2+},Gd^{3+} radii, and tetrahedrally-coordinated O^{2-} radius tabulated by Shannon (1976). The calculated BVS for the A2 site occupants, 1.92 vu and 2.10 vu, are

Table 5. Assigned site-occupancies, site-scattering, and mean bond lengths for heflikite.

Site	Site-occupancy	Site scattering (e^-) ref.	Site scattering (e^-) calc.	Mean bond-length (Å) ref.	Mean bond-length (Å) calc.
	Jordanów Śląski (holotype J11a)				
A1	Ca	20.0^{fix}	20.0	2.603(8)	2.55
A2	$Ca_{0.729}La_{0.048}Ce_{0.125}Pr_{0.010}Nd_{0.046}Sm_{0.012}Eu_{0.003}Gd_{0.016}Y_{0.005}$	31.6(3)	30.0	2.688(6)	2.59
M1	Al	13.3(3)	13.0	1.937(7)	1.905
M2	Al	13.0^{fix}	13.0	1.892(6)	1.905
M3	$Sc_{0.449}Fe^{2+}_{0.251}Al_{0.182}Fe^{3+}_{0.070}Mg_{0.020}Ti_{0.014}Mn_{0.010}V^{3+}_{0.005}$	19.6(3)	21.0	2.095(9)	2.077
T1	Si	14.0^{fix}	14.0	1.626(10)	1.630
T2	Si	14.0^{fix}	14.0	1.619(10)	1.630
T3	Si	14.0^{fix}	14.0	1.643(9)	1.630
	Heftetjern (cotype N5)				
A1	Ca	20.0^{fix}	20.0	2.597(5)	2.55
A2	$Ca_{0.644}La_{0.082}Ce_{0.235}Pr_{0.015}Nd_{0.021}Eu_{0.004}Gd_{0.018}$	33.8(2)	34.7	2.683(5)	2.63
M1	$Al_{0.958}Ti_{0.029}$	12.2(2)	13.1	1.937(5)	
M2	Al	13.0^{fix}	13.0	1.892(5)	1.905
M3	$Fe^{2+}_{0.434}Sc_{0.362}Fe^{3+}_{0.128}Sn_{0.029}Mn_{0.009}$	23.6(2)	23.9	2.089(6)	2.088
T1	Si	14.0^{fix}	14.0	1.626(7)	1.630
T2	Si	14.0^{fix}	14.0	1.616(7)	1.630
T3	Si	14.0^{fix}	14.0	1.643(6)	1.630

Notes: 'fix' – a fixed value by the fixed site occupancy. Mean bond lengths were calculated on the basis of the empirical formulae and respective cation radii and O^{2-} anion radius by Shannon (1976).

Table 6. Bond-valence analysis (in valence units) for heflikite.*

Jordanów Śląski (holotype J11a)										
	A1	A2	M1	M2	M3	T1	T2	T3	H10	BVS_a
O1	0.28 $^{\times2\downarrow}$		0.42 $^{\times2\downarrow}$		0.30 $^{\times2\downarrow}$	0.96 $^{\times2\downarrow}$				1.96
O2		0.15 $^{\times2\downarrow}$			0.44 $^{\times2\downarrow}$			1.00 $^{\times2\downarrow}$	0.03 $^{\times2\downarrow\times2\rightarrow}$	1.89
		0.25 $^{\times2\downarrow}$								
O3	0.35 $^{\times2\downarrow}$	0.15 $^{\times2\downarrow}$		0.56$^{\times2\downarrow}$			1.00 $^{\times2\downarrow}$			2.05
O4			0.57 $^{\times2\downarrow\times2\rightarrow}$		0.52				0.08	1.73
O5	0.20		0.41 $^{\times2\downarrow\times2\rightarrow}$					0.88		1.89
O6	0.09			0.47 $^{\times2\downarrow\times2\rightarrow}$				0.94		1.96
O7	0.34	0.46				1.09				1.89
O8		0.07 $^{\times2\downarrow\times2\rightarrow}$			0.64		1.04			1.83
O9	0.06$^{\times2\downarrow}$					0.97	1.01			2.04
O10		0.22		0.53 $^{\times2\downarrow\times2\rightarrow}$					0.88	2.16
BVS_c	2.01	1.92	2.79	3.10	2.63	3.99	4.05	3.81	1.01	
MFV	2.00	2.25	3.00	3.00	2.74	4.00	4.00	4.00	1.00	

Heftetjern (cotype N5)										
	A1	A2	M1	M2	M3	T1	T2	T3	H10	BVS_a
O1	0.28 $^{\times2\downarrow}$		0.42 $^{\times2\downarrow}$		0.31 $^{\times2\downarrow}$	0.95 $^{\times2\downarrow}$				1.96
O2		0.17 $^{\times2\downarrow}$			0.42 $^{\times2\downarrow}$			0.99 $^{\times2\downarrow}$	0.02 $^{\times2\downarrow\times2\rightarrow}$	1.91
		0.29 $^{\times2\downarrow}$								
O3	0.36 $^{\times2\downarrow}$	0.15 $^{\times2\downarrow}$		0.55$^{\times2\downarrow}$			1.03 $^{\times2\downarrow}$			2.09
O4			0.56 $^{\times2\downarrow\times2\rightarrow}$		0.53				0.08	1.74
O5	0.21		0.41 $^{\times2\downarrow\times2\rightarrow}$					0.90		1.92
O6	0.09			0.48 $^{\times2\downarrow\times2\rightarrow}$				0.94		1.98
O7	0.34	0.48				1.15				1.97
O8		0.08 $^{\times2\downarrow\times2\rightarrow}$			0.64		1.03			1.83
O9	0.06 $^{\times2\downarrow}$					0.95	0.99			2.00
O10		0.24		0.52 $^{\times2\downarrow\times2\rightarrow}$					0.89	2.17
BVS_c	2.05	2.10	2.79	3.10	2.62	4.00	4.08	3.82	1.01	
MFV	2.00	2.41	2.99	3.00	2.47	4.00	4.00	4.00	1.00	

*Notes: Bond valences were calculated using the equation $S = \exp[(R_0–R)/B]$, where R_0 and B are bond-valence parameters by Gagné and Hawthorne (2015), and R is the refined bond length; BVS_a, BVS_c – bond-valence sums over anions and cations; MFV – mean formal valence.

slightly lower than the mean formal valence of cations occupying the site (2.25 vu and 2.41 vu in the holotype and cotype, respectively), most probably owing to enlarged A2–O8 bonds (Tables 4 and 6).

Among the three types of octahedral M sites, the M2 site is occupied solely by Al. Therefore, the M1 and M3 site populations are critical for the classification of epidote-supergroup minerals. In both refined crystals the edge-sharing $M2O_6$ octahedra are very regular [quadratic elongation <λ> (Robinson *et al.*, 1971) is equal to 1.0054 and 1.0051, respectively], with M2–O bond lengths ranging from 1.862(7)–1.866(5) Å to 1.924(4)–1.932(6) Å, and <M2–O> of 1.892(4–6) Å, typical for $^{VI}Al^{3+}$–O bond (Table 4). The BVS of 3.10 vu calculated for Al as the M2 site occupant corroborates this site assignment (Table 6).

The occupancy of the M1 site was fixed as $Al_{1.00}$ for the holotype and refined as $Al_{0.940(16)}$ for the cotype crystal (Table 3).

Table 7. Structural comparison of the epidote-group minerals.

Species	Formula	*a* (Å)	*b* (Å)	*c* (Å)	β (°)	*V* (Å^3)	Refs*
Clinozoisite	$(CaCa)(AlAlAl)(Si_2O_7)(SiO_4)O(OH)$	8.879(5)	5.583(5)	10.155(6)	115.50(5)	454.36	[1]
		8.870(1)	5.592(1)	10.144(2)	115.4(2)	454.3(2)	[2]
Mukhinite	$(CaCa)(AlAlV^{3+})(Si_2O_7)(SiO_4)O(OH)$	8.90	5.61	10.15	115.50	457.41	[3]
		8.8971(11)	5.6221(6)	10.1519(11)	115.169(14)	459.60(11)	[4]
Epidote	$(CaCa)(AlAlFe^{3+})(Si_2O_7)(SiO_4)O(OH)$	8.914(9)	5.640(3)	10.162(9)	115.4(2)	461.51	[5]
		8.8877(18)	5.6275(8)	10.1517(12)	115.383(14)	458.73	[6]
		8.8802(10)	5.6043(8)	10.1511(13)	115.455(12)	456.15	[6]
Piemontite	$(CaCa)(AlAlMn^{3+})(Si_2O_7)(SiO_4)O(OH)$	8.878(10)	5.692(5)	10.201(10)	115.40(20)	466.24	[7]
Heflikite	$(CaCa)(AlAlSc)(Si_2O_7)(SiO_4)O(OH)$	8.9383(9)	5.6830(5)	10.1903(10)	115.43(12)	468.97(9)	[8]
Niigataite	$(CaSr)(AlAlAl)(Si_2O_7)(SiO_4)O(OH)$	8.890(4)	5.5878(18)	10.211(4)	115.12(3)	459.26	[9]
Epidote-(Sr)	$(CaSr)(AlAlFe^{3+})(Si_2O_7)(SiO_4)O(OH)$	8.928(5)	5.652(1)	10.244(5)	114.46(4)	470.5	[10]
Piemontite-(Sr)	$(CaSr)(AlAlMn^{3+})(Si_2O_7)(SiO_4)O(OH)$	8.8942(1)	5.6540(1)	10.1928(1)	115.100(1)	464.17	[11]
Tweddillite	$(CaSr)(Mn^{3+}AlMn^{3+})(Si_2O_7)(SiO_4)O(OH)$	8.932(5)	5.698(4)	10.310(5)	114.56(4)	477.25	[12]
Hancockite	$(CaPb)(AlAlFe^{3+})(Si_2O_7)(SiO_4)O(OH)$	8.958(20)	5.665(10)	10.304(20)	114.4(4)	476.19	[5]
		8.9496(3)	5.6474(2)	10.2724(3)	114.362(1)	472.96	[13]
Piemontite-(Pb)	$(CaPb)(AlAlMn^{3+})(Si_2O_7)(SiO_4)O(OH)$	8.938(1)	5.6810(6)	10.289(1)	114.17(1)	476.64	[14]

*References: [1] Dollase (1968); [2] Comodi and Zanazzi (1997); [3] Shepel and Karpenko (1969); [4] Korinevsky *et al.* (2022); [5] Dollase (1971); [6] Gabe *et al.* (1973); [7] Dollase (1969); [8] this paper; [9] Miyajima *et al.* (2003); [10] Minakawa *et al.* (2008); [11] Bonazzi *et al.* (1990); [12] Armbruster *et al.* (2002); [13] Perchiazzi *et al.* (2022); [14] Chukanov *et al.* (2012).

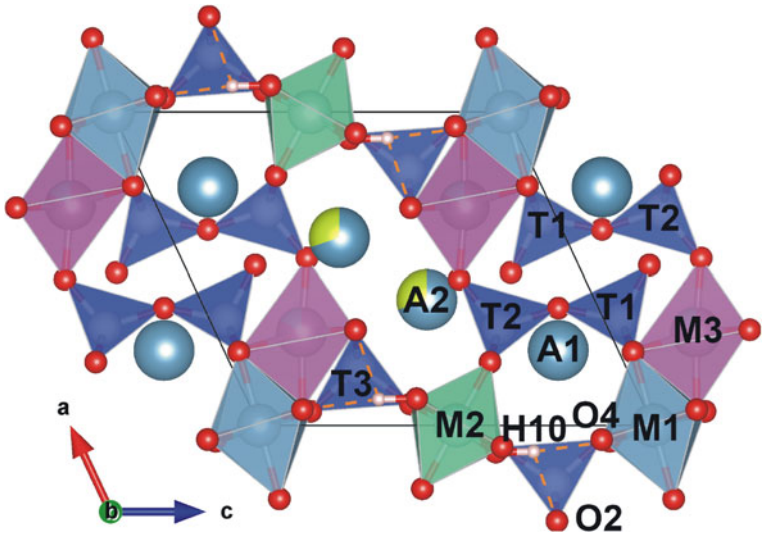

Figure 4. Crystal structure of heflikite, view along **b**. Thin orange dashed lines denote hydrogen bonds O10–H···O2 and O10–H···O4. Figure prepared with *VESTA* Version 3 (Momma and Izumi, 2011).

Thus, for the holotype it may be considered that the M1 site is filled only by Al^{3+}. For the cotype the refined M1 site-occupancy suggests a small deficit, which can be partly compensated by Ti^{4+} according to the suggestion of Armbruster *et al.* (2006). However, the analysis of the refined M1–O bond lengths indicates distinctly enlarged M1–O1 and M1–O5 bonds compared to the M1–O4 bond, 1.971(5)–1.984(7) Å vs 1.855(6)–1.857(5) Å, and distinctly increased refined <M1–O> up to 1.937 Å for both crystals (quadratic elongation <λ> = 1.0057 and 1.0058, Table 4). In consequence, the calculated BVS for the site occupant(s) are lowered to 2.79 vu, although the virtual valence of the M1 site occupant (Al or Al + Ti) is ~3+ (Table 6).

The $M3O_6$ octahedron is attached to the $M1O_6$-octahedra chain by two O1–O4 common edges. The M3 site occupancy was refined as $Sc_{0.83(4)}Al_{0.17(4)}$ for the holotype and $Sc_{0.48(4)}Fe_{0.52(4)}$ for the cotype (Table 3). These occupancies indicate the M3 site population with 19.6(3) e^- in the holotype and 23.6(2) e^- in the cotype (Table 5). Considering accuracies of the EPMA, these values correspond well to the numbers of electrons at the site, respectively 21.0 e^- and 24.5 e^-, derived from the empirical formulae. The $M3O_6$ octahedron shows the strongest deformation (<λ> = 1.0309 in both crystals) with M3–O distances ranging from 1.913(13)–1.914(8) Å to 2.248(8)–2.225(5) Å. The refined <M3–O>, 2.095(9) Å for holotype and 2.089(6) Å for cotype, correspond well to the values of 2.077 Å and 2.088 Å derived from the empirical formulae using the respective cation radii and O^{2-} radius from Shannon (1976) (Table 6). Similarly to the M1 site, a slightly decreased BVS of 2.62–2.63 vu *versus* 2.73 and 2.47 vu means formal valence of the M3 cation may result from the enlargement of the M3–O bonds. Heflikite, with the largest trivalent M3 site occupant, has the highest unit-cell volume of all the epidote-group species with $^{A1}Ca^{A2}Ca$ and $^{M1}Al^{M2}Al$, except the species containing Sr^{2+} or Pb^{2+} at the A2 site (Table 7).

Calculated powder XRD data

Powder XRD data could not be collected owing to the scarcity and heterogeneity of the heflikite crystals. Therefore, the powder pattern was calculated from the refined single-crystal structure of holotype heflikite using the *PowderCell 2.4* software (Nolze and Kraus, 1998). The seven strongest reflections [*d* in Å (*I*) *hkl*] are as follows: 3.513 (41.0) $\bar{2}11$; 2.913 (100) $\bar{1}13$; 2.842 (40.8) 020; 2.706 (31.0) 013; 2.681 (22.6) 120; 2.617 (46.1) $\bar{3}11$; 2.412 (21.9) $\bar{3}13$. The complete calculated powder XRD data has been deposited with the Principal Editors of *Mineralogical Magazine* and is available as Supplementary material (S3).

Raman spectroscopy

The Raman spectrum of heflikite was recorded from the core of the compositionally-zoned crystal J11c in the holotype sample (Fig. 1c,d) in back-scattered geometry with a Horiba Labram HR spectrometer integrated with an Olympus BX 41 confocal microscope. The domain of this crystal is highly enriched in Sc and has the following composition (Table S1):

$$^{A1}Ca^{A2}(Ca_{0.756}Ce_{0.122}La_{0.046}Nd_{0.043}Gd_{0.014}Pr_{0.011}Sm_{0.010}Eu_{0.003}Y_{0.001})_{\Sigma 1.006}\ ^{M1}Al_{0.990}\ ^{M2}Al^{M3}[(Sc_{0.526}Al_{0.179}V^{3+}_{0.009}Fe^{3+}_{0.005})_{\Sigma 0.719}(Fe^{2+}_{0.248}Mg_{0.011}Mn_{0.005})_{\Sigma 0.264}\ Ti_{0.017}]_{\Sigma 1.000}(Si_{3.006}O_{11})O(OH).$$

The system was calibrated using the Rayleigh line. The spectrum was recorded on a random section of the crystal hosted in a pegmatitic matrix mounted in epoxy resin in the range of 50–4000 cm^{-1} using the 532 nm line of a solid-state Nd–YAG laser (10 mW) and 1800 grating. The Raman measurements were carried out using two accumulated scans per spectrum, each scan with an acquisition time of 600 s, an objective with 100× magnification, the minimum lateral and depth resolution of ~1 μm, and an estimated analytical spot size of ~3–5 μm. The deconvolution of the spectrum was done with the *FITYK-1.3.1* software (Wojdyr, 2010) in the ranges of 50–1200 cm^{-1} and 3000–4000 cm^{-1}. To remove the effect of luminescence, the linear background was removed in the first spectral range while in the second range the spectrum was processed without the background removal. Component bands have been added to the fitting model using the auto-add peak mode in such a way to minimise the difference between the empirical spectrum and the theoretical spectrum. Spectral position and intensities of the component bands were anticipated on the basis of the shape of the empirical spectrum (peaks maxima, asymmetry of the peaks and inflections on the peaks shoulders). The input model was fitted with Voigt function applying the Levenberg–Marquardt fitting method (Levenberg, 1944; Marquardt, 1963).

Compared to the RRUFF database (Lafuente *et al.*, 2015), the Raman spectrum of heflikite corresponds well to the spectra of

clinozoisite (R040085) and epidote (R050202) and is significantly different from that of allanite-(Ce) (R080044) (Fig. 5a). The deconvolution revealed 25 component bands in the Raman shift range of 50–1200 cm^{-1} centred at (s – strong, m – moderate, w – weak): (s) 101, 452, 568, 682 and 975 cm^{-1}; (m) 128, 281, 385, 425, 489, 514, 605, 875, 912, 963 and 1061 cm^{-1}; (w) 147, 240, 306, 326, 361, 632, 689, 832 and 1021 cm^{-1} (Fig. 5b).

In general, Raman spectra of the epidote-supergroup minerals remain poorly understood. Nagashima *et al.* (2021) observed that substitutions at the M sites of the epidote structure can significantly influence the geometry of SiO_4 and Si_2O_7 units. Therefore, unambiguous interpretation of the spectral range below 1250 cm^{-1} is difficult owing to the presence of multiple overlapping bands. For the same reason, precise assignment of Raman bands is also difficult in the case of heflikite. Some Raman bands correspond closely to the bands observed in the spectra of clinozoisite and epidote (e.g. Liebscher, 2004; Limonta *et al.*, 2022; Nagashima and Mihailova, 2023, and references therein) but most of them occur at slightly different wavenumbers owing to differences in the site occupancies among these minerals. According to Nagashima *et al.* (2021), the most intense Raman band at 975 cm^{-1} in the spectrum of heflikite can be assigned to the Si–O stretching mode, the band at 568 cm^{-1} to the Si–O–Si bending mode, and the features in the

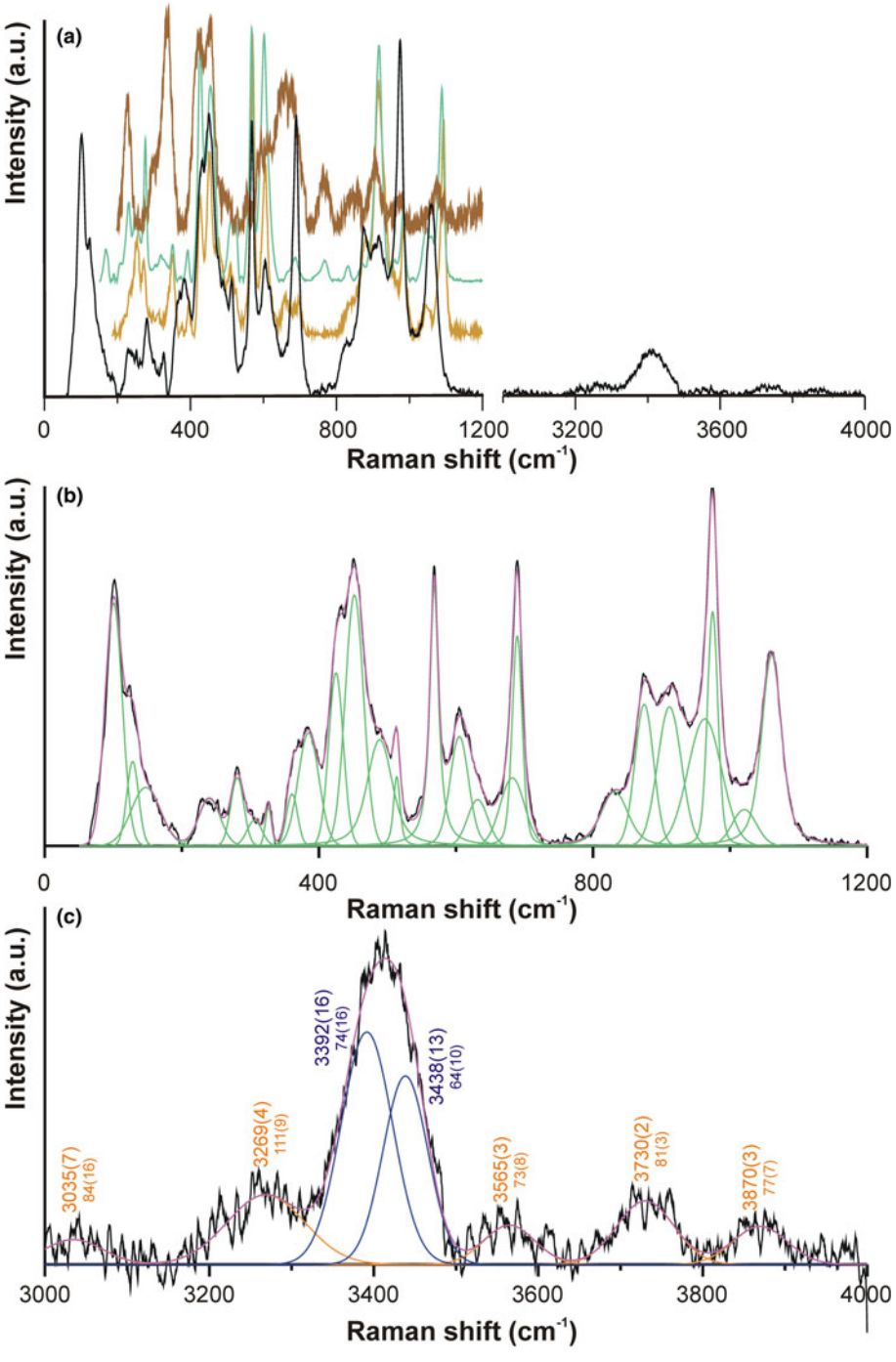

Figure 5. Raman spectrum of heflikite (black): (a) compared with the spectra of clinozoisite R040085 (green), epidote R050202 (yellow) and allanite-(Ce) R080044 (brown) from the RRUFF database; (b) deconvolution of the spectrum in the lattice vibration region 50–1200 cm^{-1}. Line colours: black – recorded spectrum, green – component bands, magenta – fitted spectrum; (c) deconvolution of the spectrum in the OH stretching vibration region 3000–4000 cm^{-1}. Line colours: black – recorded spectrum, magenta – fitted spectrum, yellow – luminescence bands, blue – OH bands related to ^{M3}Sc. Parameters of the component bands: first number – band position, second number – full width at half maximum, numbers in parentheses indicate standard errors.

regions around 100 cm^{-1} and 240 cm^{-1} are most probably connected to heavy-cation vibrations and external silicate modes. Varlamov *et al.* (2019) assigned bands from the range 300–600 cm^{-1} collectively to the M–O stretching vibrations and bending vibrations of silicate anions. In their studies on various epidote-supergroup minerals, Varlamov *et al.* (2019) assigned the band in the range of 1020–1200 cm^{-1} to stretching vibrations of the Si–O–Si bridges. They also agreed with the suggestion of Chukanov (2014) that its exact spectral position depends on the Si–O–Si angle in such a way that a higher value of the angle is reflected by a higher frequency of the corresponding vibration. In the Raman spectrum of heflikite, the band is centred at 1061 cm^{-1}. This falls between the ranges of 1074–1078 cm^{-1} and 1024–1056 cm^{-1}, which were identified by Varlamov *et al.* (2019) as typical for REE-free and REE-bearing epidote-supergroup minerals, respectively. This spectral position correlates well with the refined ^{T1}Si–O9–^{T2}Si angle of 151.4(9)° in heflikite, the value intermediate between those found in the structures of ferriallanite-(La), 143.61° (Kolitsch *et al.*, 2012) and epidote, 154.59° (Gatta *et al.*, 2010) and 155.45(8)° (Gatta *et al.*, 2012), and also agrees with a subordinate content of the allanite component in the holotype heflikite.

Previous studies of the O–H stretching region using infrared and Raman spectroscopy revealed that O–H bond stretching signals in epidote-group minerals are complex, comprising overlapping, strongly pleochroic bands. The exact position of the band is dependent on the amount of trivalent cations, such as Fe^{3+}, Mn^{3+}, Cr^{3+} and V^{3+}, substituting for Al at the octahedral sites. The positive relationship between the concentration of Fe in the clinozoisite–epidote solid-solution series and the wavenumber of the bands' maxima has been firmly established (e.g. Langer and Raith, 1974; Della Ventura *et al.*, 1996; Liebscher, 2004; Gatta *et al.*, 2012; Nagashima *et al.*, 2021; Limonta *et al.*, 2022; Nagashima and Mihailova, 2023). In the Raman spectra of clinozoisite–epidote minerals, the position of the O–H stretching peak typically varies from ~3340 cm^{-1} in Fe-poor crystals to ~3390 cm^{-1} in Fe-rich species (e.g. Limonta *et al.*, 2022; Nagashima and Mihailova, 2023). Aside from this shift, a split of the O–H stretching band in piemontite is observed, caused by the Jahn–Teller effect related to the presence of Mn^{3+} (Della Ventura *et al.*, 1996; Liebscher, 2004). The O–H stretching region in the Raman spectrum of the heflikite holotype contains a broad and slightly asymmetric band of moderate intensity, centred at ~3412 cm^{-1} (Fig. 5c). The spectral position of the band can be modelled at 3411.2(8) with FWHM = 92(2) cm^{-1}. However, the J11c crystal is poor in Fe^{3+} (with almost no Fe^{3+} in the core), and on the basis of its M1–M3 site populations, it is evident that the high wavenumber of the OH stretching band is due to the presence of a significant amount of Sc^{3+} at the M3 site.

Possible M3 site occupants exhibit significant differences in their cation radii as r_{Al3+} = 0.535 Å, r_{Fe3+} = 0.645 Å, and r_{Sc3+} = 0.745 Å (according to Shannon, 1976). The replacement of elements at the M3 site not only affect the M3–O bond lengths and respective bond valences, but also other bond lengths and bond valences in which oxygen atoms coordinated by the M3 cations participate, such as the M1–O4 bond, and the H^+ of the ^{O10}O–H hydroxyl. The hydrogen atom, which is bonded to the O10 oxygen (acting as a donor), is involved in two hydrogen bonds. These are with the O4 and the O2 atoms acting as acceptors. In a Fourier-transform infrared spectrum of epidote (Gatta *et al.*, 2012) and a Raman spectrum of synthetic clinozoisite (Nagashima *et al.*, 2021), the hydrogen bond O10–H···O4 was stronger than O10–H···O2, and the O10–H bond stretching mode appeared at lower wavenumbers for O10–H···O4 (~3350–3385 cm^{-1}) than for O10–H···O2 (~3400 cm^{-1}). This is because the M3–O2 and M3–O4 distances increase more rapidly than M2–O10, proportionally with the replacement of ^{M3}Al in clinozoisite by Fe^{3+} in epidote (and especially Sc^{3+} in heflikite) due to the increasing mean radius of the M3 site occupant. The deconvolution of the OH stretching range 3000–4000 cm^{-1} in heflikite (Fig. 5c) reveals the presence of several component bands, including two with still acceptable statistical parameters related to hydrogen bonds O10–H···O2 and O10–H···O4. The strength of the O10–H···O4 bond was found to be greater compared to the O10–H···O2 bond (0.08 vu *versus* 0.02–0.03 vu), as indicated by the configuration of both types of hydrogen bonds (Table 6). In consequence, the O10–H···O4 stretching mode, which corresponds to the $^{M1,2}Al_2$–O10–H···O4–$^{M1,2}Al_2{}^{M3}$(Sc,Al) arrangement, appears at a lower wavenumber [3392(16) cm^{-1}] compared to the O10–H···O2 stretching mode corresponding to the $^{M1,2}Al_2$–O10–H···O2–$^{M1,2}Al_2{}^{M3}$(Sc,Al) arrangement [3438(13) cm^{-1}]. When comparing the results for heflikite with those obtained by Gatta *et al.* (2012) for epidote and by Nagashima *et al.* (2021) for synthetic clinozoisite, it becomes apparent that replacing $^{M3}Al^{3+}$ with Fe^{3+} and Sc^{3+} results in an increase of the <M3–O> distance, leading to a gradual weakening of both types of hydrogen bonds. Relatively strong bonds in $^{M1,2}Al_2$–O10–H···O4–$^{M1,2}Al_2{}^{M3}$Al and $^{M1,2}Al_2$–O10–H···O2–$^{M1,2}Al_2{}^{M3}$Al arrangements weaken within $^{M1,2}Al_2$–O10–H···O4–$^{M1,2}Al_2{}^{M3}Fe^{3+}$ and $^{M1,2}Al_2$–O10–H···O2–$^{M1,2}Al_2{}^{M3}Fe^{3+}$ configurations, and diminish further in $^{M1,2}Al_2$–O10–H···O4–$^{M1,2}Al_2{}^{M3}$Sc and $^{M1,2}Al_2$–O10–H···O2–$^{1,2}Al_2{}^{M3}$Sc. At the same time, the strength of the corresponding O10–H bond increases. The changes in the occupancy of the M3 site result in a splitting of the O–H stretching bands and a shift of the component bands towards higher wavenumbers.

Other very weak bands in the OH stretching vibration region of the Raman spectrum of heflikite cannot be interpreted unambiguously. They most probably represent luminescence [3035(7), 3269(4), 3565(3), 3730(2) and 3870(3) cm^{-1}]. A slightly enhanced band at 3269(4) cm^{-1} could also be related to OH vibrations coupled to lattice vibrations as suggested by Gatta *et al.* (2012), while bands in the range of 3500–4000 cm^{-1} can be assigned to OH groups participating in allanite-type arrangements with divalent octahedral occupants at the M3 site, mainly Fe^{2+} (Limonta *et al.*, 2022; fig. 4).

Genetic implications

Scandium mineralisation is currently of great interest to industry and technology due to the rapidly growing demand from manufacturers of high-tech aluminium alloys, solid oxide fuel cells, solid-state lasers, and other applications. REE-poor epidote-supergroup minerals have not previously been considered as a possible source of Sc. Reports on specimens with significant Sc enrichment are rare and limited to REE-enriched species (Meyer, 1911; Foord *et al.* 1993; Raade and Kristiansen, 2000; Kristiansen, 2009; Čopjaková *et al.*, 2015). Here, we report the discovery of heflikite, $Ca_2(Al_2Sc)(Si_2O_7)(SiO_4)O(OH)$, a new and the only Sc-rich epidote-supergroup mineral. Heflikite is closely related to clinozoisite and epidote, both widespread in various geological environments, through isovalent substitutions $^{M3}Sc^{3+} \rightarrow {}^{M3}Al$ and $^{M3}Sc^{3+} \rightarrow {}^{M3}Fe^{3+}$, respectively. The mode of occurrence and textural position of the holotype and cotype heflikite indicate its formation from hydrothermal fluids at low to moderate temperatures and pressures. In

the Heftetjern pegmatite, it is a part of a diverse assemblage of late-stage hydrothermal Sc minerals, including bazzite, cascandite, heftetjernite, kristiansenite, oftedalite, scandiobabingtonite and thortveitite (Raade *et al.*, 2002; Kristiansen, 2009; Chukanov *et al.*, 2017; Steffenssen *et al.*, 2020). The granitic pegmatite at Jordanów Śląski also hosts Sc-rich minerals, such as Sc-rich ixiolite, cascandite, kristiansenite, bazzite, Sc-rich actinolite (Pieczka *et al.*, 2024a), and scandio-winchite (Pieczka *et al.*, 2024b). They formed from metasomatic fluids that infiltrated a contact between the granitic pegmatite and the surrounding rodingite-type calc-silicate rocks and serpentinites, introducing Sc into the pegmatite. The fluids could have either been hydrothermal or related to low-grade regional metamorphism that postdated the formation of the pegmatite. The stability field of heflikite and extents of its solid solution with other epidote-group minerals require further examination. Nonetheless, although heflikite has only been discovered in a few small crystals, it still demonstrates that the epidote-group minerals can act as effective collectors for scandium.

Acknowledgements. The authors thank Peter Leverett and two anonymous reviewers for their very helpful comments and suggestions, which greatly improved the manuscript. We also thank Mr. O.T. Ljøstad, Elverum, Norway, for permission to use his photograph of allanite-(Ce) – Sc-rich epidote crystals from Heftetjern. This study was supported by the National Science Centre (Poland) grant 2019/33/B/ST10/00120 to A.P.

Supplementary material. The supplementary material for this article can be found at https://doi.org/10.1180/mgm.2023.98.

Competing interests. The authors declare none.

References

Armbruster T., Gnos E., Dixon R., Gutzmer J., Hejny C., Dobelin N. and Medenbach O. (2002) Manganvesuvianite and tweddillite, two new Mn^{3+}-silicate minerals from the Kalahari manganese fields, South Africa. *Mineralogical Magazine*, **66**, 137–150.

Armbruster T., Bonazzi P., Akasaka M., Bermanec V., Chopin Ch., Gieré R., Heuss-Assbichler S., Liebscher A., Menchetti S., Pan Y. and Pasero M. (2006) Recommended nomenclature of epidote-group minerals. *European Journal of Mineralogy*, **18**, 551–567.

Awdankiewicz M., Kryza R., Turniak K., Ovtcharova M. and Schaltegger U. (2021) The Central Sudetic Ophiolite (European Variscan Belt): Precise U–Pb zircon dating and geotectonic implications. *Geological Magazine*, **158**, 555–566.

Bergstøl S. and Juve G. (1988) Scandian ixiolite, pyrochlore and bazzite in granite pegmatite in Tørdal, Telemark, Norway. A contribution to the mineralogy and geochemistry of scandium and tin. *Mineralogy and Petrology*, **38**, 229–243.

Bonazzi P., Menchetti S. and Palenzona A. (1990) Strontiopiemontite, a new member of the epidote group, from Val Graveglia, Liguria, Italy. *European Journal of Mineralogy*, **2**, 519–523.

Chukanov N.V. (2014) *Infrared Spectra of Mineral Species: Extended Library*. Springer-Verlag, Dordrecht–Heidelberg–New York–London.

Chukanov N.V., Varlamov D.A., Nestola F., Belakovskiy D.I., Goettlicher J., Britvin S.N., Lanza A. and Jancev S. (2012) Piemontite-(Pb), $CaPbAl_2Mn^{3+}[Si_2O_7][SiO_4]O(OH)$, a new mineral species of the epidote supergroup. *Neues Jahrbuch für Mineralogie-Abhandlungen, Journal of Mineralogy and Geochemistry*, **189**, 275–286.

Chukanov N.V., Aksenov S.A., Rastsvetaeva R.K., Kristiansen R., Pekov I.V., Belakovskiy D.I., Van K.V., Bychkova Y.V. and Britvin S.N. (2017) Crystal structure of the OH-dominant gadolinite-(Y) analogue $(Y,Ca)_2(Fe,\square)Be_2Si_2O_8(OH,O)_2$ from Heftetjern pegmatite, Norway. *Acta Crystallographica*, **B73**, 899–906.

Comodi P. and Zanazzi P.F. (1997) The pressure behavior of clinozoisite and zoisite: An X-ray diffraction study. *American Mineralogist*, **82**, 61–68.

Cooper M.A., Hawthorne F.C., Ball N.A., Černý P. and Kristiansen R. (2006) Oftedalite, $(ScCa,Mn_2^{2+})KBe_3Si_{12}O_{30}$, a new mineral species of the milarite group from the Heftetjern pegmatite, Tørdal, Norway: description and crystal structure. *The Canadian Mineralogist*, **44**, 943–949.

Cooper M.A., Hawthorne F.C., Miyawaki R. and Kristiansen R. (2019) Cation order in the crystal structure of 'Ca-hingganite-(Y)'. *The Canadian Mineralogist*, **57**, 371–382.

Čopjaková R., Škoda R., Vašinová Galiová M., Novák M. and Cempírek J. (2015) Sc- and REE-rich tourmaline replaced by Sc-rich REE-bearing epidote-group mineral from the mixed (NYF + LCT) Kracovice pegmatite (Moldanubian Zone, Czech Republic). *American Mineralogist*, **100**, 1434–1451.

Della Ventura G., Mottana A., Parodi G.C. and Griffin W.L. (1996) FTIR spectroscopy in the OH-stretching region of monoclinic epidotes from Praborna (St. Marcel, Aosta Valley, Italy). *European Journal of Mineralogy*, **8**, 655–665.

Dollase W.A. (1968) Refinement and comparison of the structures of zoisite and clinozoisite. *American Mineralogist*, **53**, 1882–1898.

Dollase W.A. (1969) Crystal structure and cation ordering of piemontite. *American Mineralogist*, **54**, 710–717.

Dollase W.A. (1971) Refinement of the crystal structures of epidote, allanite and hancockite *American Mineralogist*, **56**, 447–464.

Dolomanov O.V., Bourhis L.J., Gildea R.J., Howard J.A.K. and Puschmann H. (2009) OLEX2: a complete structure solution, refinement and analysis program. *Journal of Applied Crystallography*, **42**, 339–341.

Dubińska E. (1995) Rodingites of the eastern part of the Jordanów – Gogołów serpentinite massif, Lower Silesia, Poland. *The Canadian Mineralogist*, **33**, 585–608.

Dubińska E. (1997) Rodingites and amphibolites from the serpentinites surrounding Góry Sowie block (Lower Silesia, Poland): record of suprasubduction zone magmatism and serpentinization. *Neues Jahrbuch für Mineralogie, Abhandlungen*, **171**, 239–279.

Dubińska E. and Szafranek D. (1990) On the origin of layer silicates from Jordanów (Lower Silesia, Poland). *Archiwum Mineralogiczne*, **46**, 19–36.

Dubińska E. and Wiewióra A. (1988) Layer silicates in the contact zone between granite and serpentinite, Jordanów, Lower Silesia, Poland. *Clay Minerals*, **23**, 459–470.

Dubińska E., Bylina P., Kozłowski A., Dörr W., Nejbert K., Schastok J. and Kulicki C. (2004) U–Pb dating of serpentinization: hydrothermal zircon from a metasomatic rodingite shell (Sudetic ophiolite, SW Poland). *Chemical Geology*, **203**, 183–203.

Foord E.E., Birmingham S.D., Demartin F., Pilati T., Gramaccioli C.M. and Lichte F.E. (1993) Thortveitite and associated Sc-bearing minerals from Ravalli County, Montana. *The Canadian Mineralogist*, **31**, 337–346.

Frei D., Liebscher A., Franz G. and Dulski P. (2004) Trace element geochemistry of epidote minerals. Pp. 553–605 in: *Epidotes* (Axel Liebscher and Gerhard Franz, editors). Reviews in Mineralogy & Geochemistry, **56**. Mineralogical Society of America and the Geochemical Society, Chantilly, Virginia, USA.

Gabe E.J., Portheine J.C. and Whitlow S.H. (1973) A reinvestigation of the epidote structure: confirmation of the iron location. *American Mineralogist*, **58**, 218–223.

Gagné O.C. and Hawthorne F.C. (2015) Comprehensive derivation of bond-valence parameters for ion pairs involving oxygen. *Acta Crystallographica*, **B71**, 562–578.

Gaines R.V., Skinner H.C., Foord E.E., Mason B. and Rosenzweig A. (1997) *Dana's New Mineralogy*. Eighth Edition. John Wiley & Sons, Inc, 1819 pp.

Gatta G.D., Meven M. and Bromiley G. (2010) Effects of temperature on the crystal structure of epidote: a neutron single-crystal diffraction study at 293 and 1070 K. *Physics and Chemistry of Minerals*, **37**, 475–485.

Gatta G.D., Alvaro M. and Bromiley G. (2012) A low temperature X-ray single-crystal diffraction and polarised infra-red study of epidote. *Physics and Chemistry of Minerals*, **39**, 1–15.

Gil G. (2013) Petrographic and microprobe study of nephrites from Lower Silesia (SW Poland). *Geological Quarterly*, **57**, 395–404.

Gil G., Barnes J.D., Boschi C., Gunia P., Szakmány G., Bendő Z., Raczynski P. and Péterdi B. (2015) Origin of serpentinite-related nephrite from Jordanów and adjacent areas (SW Poland) and its comparison with selected nephrite occurrences. *Geological Quarterly*, **59**, 457–472.

Gil G., Bagiński B., Gunia P., Madej S., Sachanbiński M., Jokubauskas P. and Belka Z. (2020) Comparative Fe and Sr isotope study of nephrite deposits hosted in dolomitic marbles and serpentinites from the Sudetes, SW Poland: implications for Fe-As-Au-bearing skarn formation and post-obduction evolution of the oceanic lithosphere. *Ore Geology Reviews*, **118**, 103335.

Hawthorne F.C., Abdu Y.A., Ball N.A, Černý P. and Kristiansen R. (2014) Agakhanovite-(Y), ideally (Y,Ca)$\square_2$KBe$_3$Si$_{12}$O$_{30}$, a new milarite-group mineral from the Heftetjern pegmatite, Tørdal, Southern Norway: Description and crystal structure. *American Mineralogist*, **99**, 2084–2088.

Heflik W. (1967) *Studium mineralogiczno-petrograficzne leukokratycznej strefy przeobrażonej okolic Jordanowa Śląskiego (Dolny Śląsk)*. Prace Mineralogiczne PAN, 10, Wydawnictwa Geologiczne, 122 pp. [in Polish].

Heflik W. (1982) Petrographic position of rodingites from Jordanów (Lower Silesia). *Przegląd Geologiczny*, **6**, 277–280 [in Polish with English abstract].

Kolitsch U., Kristiansen R., Raade G. and Tillmanns E. (2010) Heftetjernite, a new scandium mineral from the Heftetjern pegmatite, Tørdal, Norway. *European Journal of Mineralogy*, **22**, 309–316.

Kolitsch U., Mills S.J., Miyawaki R. and Blass G. (2012) Ferriallanite-(La), a new member of the epidote supergroup from the Eifel, Germany. *European Journal of Mineralogy*, **24**, 741–747.

Korinevsky V.G., Chukanov N.V., Aksenov S.M., Korinevsky E.V., Kotlyarov V.A., Zamyatin D.A., Ryanskaya A.D., Kolisnichenko S.V., Lebedeva S.M. and Ermolaeva V.N. (2022) Crystal chemistry and origin of REE-bearing mukhinite from carbonate veins of the Svetlinsky gold deposit, South Urals, Russia. *Mineralogical Magazine*, **86**, 821–833.

Kristiansen R. (2009) A unique assemblage of scandium-bearing minerals from the Heftetjern pegmatite, Tørdal, south Norway. *Norsk Bergversmuseum Skrifter*, **41**, 75–102.

Kristiansen R. (2018) Nye mineralfunn fra Heftetjern-pegmatitten i Tørdal. (New mineral findings in the Heftetjern pegmatite, Tørdal). *Norsk Mineralsymposium*, **2018**, 79–92.

Kryza R. (2011) Early Carboniferous (~337 Ma) granite intrusion in Devonian (~400 Ma) ophiolite of the Central-European Variscides. *Geological Quarterly*, **55**, 213–222.

Kryza R. and Pin C. (2010) The Central-Sudetic ophiolites (SW Poland): Petrogenetic issues, geochronology and palaeotectonic implications. *Gondwana Research*, **17**, 292–305.

Lafuente B., Downs R.T., Yang H. and Stone N. (2015) The power of databases: the RRUFF project. Pp. 1–30 in: *Highlights in Mineralogical Crystallography* (T. Armbruster and R.M. Danisi, editors). De Gruyter, Berlin.

Langer K. and Raith M. (1974) Infrared spectra of Al-Fe(III)-epidotes and zoisites, $Ca_2(Al_{1-p}Fe^{3+}_p)Al_2O(OH)[Si_2O_7][SiO_4]$. *American Mineralogist*, **59**, 1249–1258.

Levenberg K. (1944) A method for the solution of certain non-linear problems in least squares. *Quarterly of Applied Mathematics*, **2**, 164–168.

Liebscher A. (2004) Spectroscopy of epidote minerals. Pp. 125–170 in: *Epidotes* (Axel Liebscher and Gerhard Franz, editors). Reviews in Mineralogy & Geochemistry, **56**. Mineralogical Society of America and the Geochemical Society, Chantilly, Virginia, USA.

Limonta M., Andò S., Bersani D. and Garzanti E. (2022) Discrimination of clinozoisite–epidote Series by Raman Spectroscopy: An application to Bengal Fan Turbidites (IODP Expedition 354). *Geosciences*, **12**, 442.

Lis J. and Sylwestrzak H. (1981) New mineral unit in leucocratic zone of Jordanów near Sobótka and its genetic significance. *Przegląd Geologiczny*, **29**, 67–71 [in Polish with English summary].

Lussier A.J., Cooper M.A., Hawthorne F.C. and Kristiansen R. (2009) Triclinic titanite from the Heftetjern granitic pegmatite, Tørdal, southern Norway. *Mineralogical Magazine*, **73**, 709–722.

Majerowicz A. (1984) Petrography and genesis of rodingites in serpentinites of the Ślęża ophiolitic group. *Geologia Sudetica*, **18**, 109–132 [in Polish with English summary].

Mandarino J.A. (1979) The Gladstone-Dale relationship. Part III. Some general applications. *The Canadian Mineralogist*, **17**, 71–76.

Mandarino J.A. (1981) The Gladstone-Dale relationship. Part IV. The compatibility concept and its application. *The Canadian Mineralogist*, **19**, 441–450.

Marquardt D. (1963) An algorithm for least-squares estimation of nonlinear parameters. *SIAM Journal of the Society for Industrial and Applied Mathematics*, **11**, 431–441.

Meyer R.J. (1911) Über einen skandiumreichen Orthit aus Finnland und den Vorgang seiner Verwitterung. *Sitzungsberichte der königlichen preussischen Akademie der Wissenschaften zu Berlin*, **105**, 379–384 [in German].

Minakawa T., Fukushima H., Nishio-Hamane D. and Miura H. (2008) Epidote-(Sr), $Ca_2Al_2Fe^{3+}(Si_2O_7)(SiO_4)O(OH)$, a new mineral from the Ananai mine, Kochi Prefecture, Japan. *Journal of the Mineralogical and Petrological Sciences*, **103**, 400–406.

Miyajima H., Matsubara S., Miyawaki R. and Hirokawa K. (2003) Niigataite, $CaSrAl_3(Si_2O_7)(SiO_4)O(OH)$: Sr-analogue of clinozoisite, a new member of the epidote group from the Itoigawa-Ohmi district, Niigata Prefecture, Japan. *Journal of Mineralogical and Petrological Sciences*, **98**, 118–129.

Miyawaki R., Yokoyama K., Matsubara S., Tsutsumi Y. and Goto A. (2008) Uedaite-(Ce), a new member of the epidote group with Mn at the A site, from Shodoshima, Kagawa Prefecture, Japan. *European Journal of Mineralogy*, **20**, 261–269.

Miyawaki R., Momma K., Yokoyama K., Shigeoka M., Matsubara S., Ito M., Nakai I. and Kristiansen R. (2015) Mn-bearing hellandite-(Y) from the Heftetjern pegmatite, Tørdal, Norway. *The Canadian Mineralogist*, **53**, 345–356.

Momma K. and Izumi F. (2011) VESTA 3 for three-dimensional visualization of crystal, volumetric and morphology data. *Journal of Applied Crystallography*, **44**, 1272–1276.

Nagashima M. and Mihailova B. (2023) Optimal Raman-scattering signal for estimating the Fe^{3+} content on the clinozoisite–epidote join. *European Journal of Mineralogy*, **35**, 267–283.

Nagashima M., Armbruster T., Nishio-Hamane D. and Mihailova B. (2021) The structural state of Finnish Cr- and V-bearing clinozoisite: insights from Raman spectroscopy. *Physics and Chemistry of Minerals*, **45**, 5.

Nolze G. and Kraus W. (1998) PowderCell 2.0 for windows. *Powder Diffraction*, **13**, 256–259.

Perchiazzi N., Mauro D., Vignola P., Zaccarini F. and Eldjarn K. (2022) Zoisite-(Pb), a new orthorhombic epidote-related mineral from the Jakobsberg Mine, Värmland, Sweden, and its relationships with hancockite. *Minerals*, **12**, 51.

Pieczka A., Kristiansen R., Stachowicz M., Dumańska-Słowik M., Gołębiowska B., Sęk M., Nejbert K., Kotowski J., Marciniak-Maliszewska B., Szuszkiewicz A., Szełęg E. and Woźniak K. (2023) Heflikite, IMA 2022-139. CNMNC Newsletter 72; *Mineralogical Magazine*, **87**, 6.

Pieczka A., Stachowicz M., Zelek-Pogudz S., Gołębiowska B., Sęk M., Nejbert K., Kotowski J., Marciniak-Maliszewska B., Szuszkiewicz A., Szełęg A., Stadnicka K.M. and Woźniak K. (2024a) Scandian actinolite from Jordanów, Lower Silesia, Poland: compositional evolution, crystal structure and genetic implications. *American Mineralogist*, **109**, 174–183, https://doi.org/10.2138/am-2022-8786.

Pieczka A., Stachowicz M., Zelek-Pogudz S., Gołębiowska B., Sęk M., Nejbert K., Kotowski J., Marciniak-Maliszewska B., Szuszkiewicz A., Szełęg A., Stadnicka K.M. and Woźniak K. (2024b) Scandio-winchite, ideally $\square$(NaCa)(Mg$_4$Sc)(Si$_8$O$_{22}$)(OH)$_2$, the first scandian amphibole from Jordanów Śląski in Lower Silesia, southwestern Poland. *American Mineralogist*, https://doi.org/10.2138/am-2023-8974

Pin C., Majerowicz A. and Wojciechowska I. (1988) Upper Palaeozoic oceanic crust in the Polish Sudetes: Nd-Sr isotope and trace element evidence. *Lithos*, **21**, 195–209.

Pouchou J.L. and Pichoir F. (1991) Quantitative analysis of homogeneous or stratified microvolumes applying the model "PAP". Pp. 31–75 in: *Electron Probe Quantitation* (K.F.J. Heinrich and D.E. Newbury, editors). Springer, Boston, USA.

Raade G. (2020) Helvine-group minerals from Norwegian granitic pegmatites and some other granitic rocks: cases of significant Sc and Sn contents. *The Canadian Mineralogist*, **68**, 367–379.

Raade G. and Bernhard F. (2003) Coexisting scandium minerals in the Heftetjern granite pegmatite. Pp. 34–35 in *International Symposium on the Mineralogy and Geochemistry of Scandium*. SCANDIUM 2003, Abstracts and Proceedings, 2. University of Oslo, Oslo.

Raade G. and Erambert M. (1999) An intergrowth of scandiobabingtonite and cascandite from the Heftetjern granite pegmatite, Norway. *Neues Jahrbuch für Mineralogie Monatshefte*, **12**, 545–550.

Raade G. and Kristiansen R. (2000) Mineralogy and geochemistry of the Heftetjern granite pegmatite, Tørdal: a progress report. *Norsk Bergverksmuseum Skrift*, **17**, 19–25.

Raade G. and Kristiansen R. (2003) Scandium as a trace element in the Heftetjern pegmatite minerals. Pp. 36–37 in *International Symposium on the Mineralogy and Geochemistry of Scandium*. SCANDIUM 2003, Abstracts and Proceedings, 2. University of Oslo, Oslo.

Raade G., Ferraris G., Gula A., Ivaldi G. and Berhard F. (2002) Kristiansenite, a new calcium-scandium-tin sorosilicate from granite pegmatite in Tørdal, Telemark, Norway. *Mineralogy and Petrology*, **75**, 89–99.

Raade G., Bernhard F. and Ottolini L. (2004) Replacement textures involving four scandium silicate minerals in the Heftetjern granitic pegmatite, Norway. *European Journal of Mineralogy*, **16**, 945–950.

Reed S.J.B. and Buckley A. (1998) Rare-earth element determination in minerals by electron-probe microanalysis: application of spectrum synthesis. *Mineralogical Magazine*, **62**, 1–8.

Rigaku Oxford Diffraction (2021) *CrysAlisPro Software system, version 1.171.40.67a*. Rigaku Corporation, Wroclaw, Poland.

Robinson K., Gibbs G.V. and Ribbe P.H. (1971) Quadratic Elongation: A quantitative measure of distortion in coordination polyhedra. *Science*, **172**, 567–570.

Rosing-Schow N., Müller A., Romer R. and Friis H. (2019) New age constraints on the formation of Sveconorwegian pegmatites. *The Canadian Mineralogist*, **57**, 787–790.

Shannon R.D. (1976) Revised effective ionic radii and systematic studies of interatomic distances in halides and chalcogenides. *Acta Crystallographica*, **A32**, 751–767.

Sheldrick G.M. (2015) Crystal structure refinement with SHELXL. *Acta Crystallographica*, **C71**, 3–8.

Shepel A.V. and Karpenko M.V. (1969) Mukhinite, a new vanadium species of epidote. *Doklady Akademii Nauk SSSR*, **185**, 1342–1345 [in Russian].

Steffenssen G., Müller A., Munnik F., Friis H., Erambert M., Kristoffersen M. and Rosing-Schow N. (2020) Unusual scandium enrichments of the Tørdal pegmatites, south Norway. Part I: Garnet as Sc exploration pathfinder. *Ore Geology Reviews*, **126**, 103729.

Strunz H. and Nickel E.H. (2001) *Strunz Mineralogical Tables, Ninth Edition*. Schweizerbart'sche Verlagsbuchhandlung, Stuttgart, Germany, 870 pp.

Varlamov D.A., Ermolaeva V.N., Chukanov N.V., Jančev S., Vigasina M.F. and Plechov P.Yu. (2019) New data on epidote-supergroup minerals: unusual chemical compositions, typochemistry, and Raman spectroscopy. *Geology of Ore Deposits*, **61**, 827–842.

Waleńczak Z. (1969) Geochemistry of minor elements dispersed in quartz (Ge, Al, Ga, Fe, Ti, Li and Be). *Archiwum Mineralogiczne*, **28**, 189–335 [in Polish with English abstract].

Warr L.N. (2021) IMA–CNMNC approved mineral symbols. *Mineralogical Magazine*, **85**, 291–320.

Wojdyr M. (2010) Fityk, a general-purpose peak fitting program. *Journal of Applied Crystallography*, **43**, 1126–1128.

Wojtulek P.M., Schulz B., Klemd R., Gil G., Dajek M. and Delura K. (2021) The Central-Sudetic ophiolites – remnants of the SSZ-type Devonian oceanic lithosphere in the European part of the Variscan Orogen. *Gondwana Research*, **105**, 343–365.